June 2018

Design, Construction, and Characterization of the University of South Florida Wind Tunnel

Jason S. Garcia
University of South Florida, jgarcia4@health.usf.edu

Design, Construction, and Characterization of the University of South Florida Wind Tunnel

by

Jason S. Garcia

A dissertation submitted in partial fulfillment
of the requirements for the degree of
Doctor of Philosophy
with a concentration in Industrial Hygiene
Department of Environmental and Occupational Health
College of Public Health
University of South Florida

Major Professor: Yehia Y. Hammad, Sc.D.
Co-Major Professor: Steven P. Mlynarek, Ph.D.
Member: Rene R. Salazar, Ph.D.
Member: Skai W. Schwartz, Ph.D.

Date of Approval:
June 19, 2018

Keywords: wind tunnel, velocity profile, turbulence intensity, fluorescent polystyrene latex spheres, fluorometry

Dedication

This dissertation is dedicated to my wife, Amy. Husbands, wives, and significant others of doctoral students do not get enough credit or recognition for the sacrifices they make during their loved ones pursuit of a dream. If it wasn't for Amy's unconditional love and support throughout the duration of this project, it may not have been completed. The rollercoaster of emotions I encountered throughout the duration of this project were often extremely difficult to bear and she was always there when I needed a beer, a laugh, a hug, a kiss, and/or a shoulder to cry on. I will forever be indebted to her. I love you Amy. We made it to the finish line.

Acknowledgments

First and foremost, I must acknowledge my committee members for their support and dedication. Dr. Yehia Hammad, my major advisor, thank you for helping design and fund the construction of our wind tunnel. I am extremely proud of it and I know that future students will benefit from its existence. Dr. Steve Mlynarek, my co-major advisor, thank you for always challenging me to look at situations from different directions. I have become a better student and researcher because of it. Dr. Rene Salazar, committee member, thank you for your advice along the way and for providing opportunities for me. Dr. Skai Schwartz, committee member, thank you for pushing me out of my comfort zone and teaching me new, challenging subject matter.

I would also like to acknowledge two other professors: Dr. Thomas Bernard and Dr. Candi Ashley. Dr. Bernard, thank you for your advice, patience, and support throughout the duration of my time here. I see how well respected you are in the field and I hope one day I will be looked at in the same light. Dr. Candi Ashley, thank you for serving as my dissertation committee chairperson and for allowing me to work with you in the Heat Stress Lab. Thank you all for sharing your knowledge and experiences. You all have my utmost respect and admiration.

A big thank you goes out to the Environmental and Occupational Health Staff including Nolan Kimball, Melinda Tyler, Cathy Silva, and Kelly Freedman. You helped make sure my posters got printed, my deadlines were met, and that I got to conferences

on time. No one will understand how very valuable all of you are to this department, college, and university.

Xiao (Sarah) Liu also deserves a thank you. Sarah, a fellow doctoral candidate in Industrial Hygiene, and I worked together to develop the analytical method and calibration curve that we both used on our respective projects. She was always willing to help, answer questions, and share experiences. I wish her the best as she will be defending her dissertation in the very near future. The fluorometer calibration curve that will be discussed was used with her permission.

Last but certainly not least, I would like to thank the National Institute for Occupational Safety and Health (NIOSH) for funding my doctoral education. It was your funding that allowed me to pursue my dream. With the knowledge and skills that I have attained, I know that I am prepared to help protect the population from exposure to environmental and occupational health hazards.

Table of Contents

List of Acronyms, Abbreviations, and Symbols

β	Open Area Ratio
BLAM	Blaustein Multi-Jet Atomizer
cfm	Cubic Feet per Minute
cm^3	Cubic Centimeters
$CV_{PM2.5}$	Coefficient of Variation for Particulate Matter 2.5 Micrometers or Smaller
CV_{PM10}	Coefficient of Variation for Particulate Matter 10.0 Micrometers or Smaller
DC	Desired Concentration
D_h	Hydraulic Duct Diameter
d_p	Particle Diameter
d_s	Screen Wire Diameter
d_v	Volume Median Diameter
F	Volume Fraction of Single Particles
FPLS	Fluorescent Polystyrene Latex Spheres
FSC	Full Scale Concentration
FSU	Fluorescent Standard Units
fpm	Feet per Minute
H	Height
Hz	Hertz
IAQ	Indoor Air Quality
in	Inch

in wg	Inches Water Gauge
IRB	Institutional Review Board
L/min	Liters per Minute
L_s	Screen Length
m	Meter
m/s	Meters per Second
µg/kg	Micrograms per Kilogram
$\mu g/m^3$	Micrograms per Cubic Meter
µl	Microliter
µm	Micrometer
mg	Milligram
mg/s	Milligrams per Second
ml	Milliliter
mm	Millimeter
ng/ml	Nanograms per Milliliter
nm	Nanometers
psi	Pound per Square Inch
psig	Pounds per Square Inch Gauge
PVC	Polyvinyl Chloride
R	Desired Singlet Ratio
RPM	Revolutions per Minute
RUV	Relative Unit Value
SD	Stairmand Disk Size

σ_g	Geometric Standard Deviation of Droplet Size Distribution
USF	University of South Florida
VAG	Vilnius Aerosol Generator
W	Width
Y	Latex Dilution Factor

List of Tables

List of Figures

List of Equations

Abstract

Much of the aerosol research completed at the University of South Florida has revolved around evaluating industrial hygiene equipment and instrumentation in environmental chambers. Data collected during these studies has provided valuable baseline data on equipment and instrument performance under calm air conditions. A newly constructed wind tunnel now allows researchers to evaluate industrial hygiene instruments under moving air conditions. Because the wind tunnel is capable of producing wind velocities that a worker could encounter in the occupational setting, researchers may gain insight into instrument performance under simulated field conditions. Because aerosols can be introduced into the new wind tunnel testing section, researchers can also challenge industrial hygiene equipment and instrumentation with aerosols in sizes ranges that are of interest in public health.

The purpose of this dissertation research was to develop a new wind tunnel to be used for aerosol research at the University of South Florida. Three specific aims had to be met for this study to be successful. They included: (1) designing a wind tunnel based on best practice information outlined in scientific literature, (2) constructing an operable wind tunnel to be used for aerosol research, and (3) characterizing wind tunnel performance by examining the wind tunnel velocity profile, turbulence intensity, and aerosol introduction/collection. The actual wind tunnel was constructed to a length of approximately 20 feet, a height of approximately 2 feet at its tallest point, and includes an entrance filter housing, a settling chamber, a contraction, a testing section, a diffuser, an

exit filter housing, a fan, and exhaust duct. All components were designed and constructed using guidelines and best practices reported in the scientific literature.

Velocity profile measurements were the first way that this wind tunnel was characterized. In order to successfully obtain measurements, the wind tunnel cross section was divided into 16 equal quadrants. Five measurements were taken for each quadrant at each wind velocity. Target wind velocities for this research were 0.5 m/s, 1.0 m/s, and 2.0 m/s. Actual average wind velocities of 0.48 m/s, 1.00 m/s, and 2.04 m/s. All were within established limits reported in the scientific literature.

Turbulence intensity measurements were the second way that this wind tunnel was characterized. In order to successfully obtain measurements, the wind tunnel cross section was divided into 16 equal quadrants. Five measurements were taken for each quadrant at each wind velocity. Wind tunnels are typically designed to have the lowest turbulence intensity possible, generally below 10%. The overall average turbulence intensities for this wind tunnel at wind velocities of 0.5 m/s, 1.0 m/s, and 2.0 m/s were 9%, 10%, and 8% respectively. Overall turbulence intensity measurements were at or below 10%.

Isokinetic sampling was the final method used to characterize this wind tunnel by collecting and detecting aerosols traveling through the wind tunnel testing section. The wind tunnel was operated at wind velocities of 0.5 m/s, 1.0 m/s, and 2.0 m/s with isokinetic sampling flow rates of 15.4 L/min, 30.9 L/min, and 61.7 L/min respectively. Monodisperse fluorescent polystyrene latex spheres were used as the test aerosol because they are uniform in size and shape and can be detected by fluorometry. The Blaustein Multi-Jet Atomizer (BLAM) was used to generate monodisperse fluorescent polystyrene latex

aerosol 0.5 µm and 2.0 µm particles from liquid suspensions. The Vilnius Aerosol Generator (VAG) was used to generate monodisperse fluorescent polystyrene latex aerosol of 6.0 µm and 12.0 µm particles from dry powders. Nitrogen gas was used for delivering test aerosols into the wind tunnel. Five experimental runs were completed for each particle size and wind velocity for a total of 60 experimental runs. Fluorescence was detected in all 60 samples with average mass concentrations ranging from 0.000050 ng/ml to 0.002703 ng/ml.

Based on velocity profile measurements, turbulence intensity measurements, and isokinetic sampling, the performance of University of South Florida wind tunnel was found to be excellent, indicating that it was designed and constructed appropriately. The wind tunnel can now successfully be used by researchers interested in evaluating industrial hygiene sampling equipment with aerosols ranging from 0.5 µm to 12.0 µm in moving air with velocities ranging from 0.5 m/s to 2.0 m/s.

Introduction

The purpose of this research study was to design, construct, and characterize the performance of a wind tunnel to be used for aerosol research. It is housed in the Breath Lab at the University of South Florida's College of Public Health. The wind tunnel is an original design with the specifications of each component made according to optimum recommended design criteria presented in the scientific literature. The wind tunnel was characterized by evaluating the velocity profile and turbulence intensity along the entire testing section. Further characterization was performed using an isokinetic sampler to capture a wide size range of monodisperse aerosol that were introduced into the test section of the wind tunnel. Fluorometry was used to determine if introduced particles were collected and detected. Because this wind tunnel is the only one that is currently available on campus, information collected during this study will serve as baseline measurements for future research experiments. In addition, the use of the wind tunnel for industrial hygiene research may give insight into instrument performance under moving air conditions.

Literature Review

The study of aerosols is extremely important in the field of industrial hygiene. Once an industrial hygienist understands how an aerosol is created and behaves, he or she can design and implement control measures to ensure it does not rise above established exposure limits thereby negatively impacting workers. Aerosols have been defined as solid particles or liquid droplets that because of their small size (0.01 to 100 µm), can remain suspended in air for a long period of time (Plog & Quinlan, 2002). They can be chemical, physical, or biological in nature. With respect to deposition in the mammalian respiratory tract, aerosols can be quite problematic if not properly controlled or eliminated. Larger particles inhaled into the respiratory tract may illicit little to no effect as they are often expelled by coughing/sneezing, removed via mucociliary action, or destroyed by the immune system. Smaller particles tend to be more problematic since they have the ability to deposit deeper in pulmonary tract. Once deep in the pulmonary tract, particulates can be difficult to clear and often cause immediate or delayed toxic effects.

Hinds (1999) explains that the human respiratory system is divided into three regions: the oropharyngeal, the tracheobronchial, and the alveolar. Particles can deposit in these regions by interception, inertial impaction, diffusion, gravitational settling, or electrostatic attraction (William C Hinds, 1999). The exact point where a particle settles is determined by its unique size, density, and geometric shape. In addition, individual human traits such as breathing rate and anatomy may further influence the exact location of particle settling. The specific sizes used in this study were 0.5, 2.0, 6.0, and 12.0 µm.

The 0.5 and 2.0 µm particles were in liquid suspension form while the 6.0 and 12.0 µm particles were a dry powder. Particles as small as 0.5 µm normally reach the alveolar region of the lung. While particles 2.0, 6.0, and 12.0 µm can reach the alveolar region, they typically deposit in the head airways or tracheobronchial region (William C Hinds, 1999). These four sizes were selected for the study because they have the ability to enter the respiratory system and cause adverse health effects.

Acute and Chronic Health Effects of Inhaled Particles

Inhaled particles can cause both acute and chronic health effects which have been investigated by the scientific community (Ayres, 2002; Brunekreef & Holgate, 2002; Kampa & Castanas, 2008; Pope III & Dockery, 2006; Seaton, Godden, MacNee, & Donaldson, 1995). Exposure to inhaled matter has a significant impact on the lungs and the heart. The United States Environmental Protection Agency explains that exposure to inhaled particulates has been associated with early death in individuals with cardiovascular or pulmonary diseases, heart attacks, asthma, decreased pulmonary function, elevated pulmonary irritation (United States Environmental Protection Agency, 2016b). While the respiratory and the cardiovascular system are greatly impacted by breathing contaminated air, the nervous system and reproductive system can also be damaged by exposure.

Many individuals are exposed to contaminated air in their home and work environment. Exposures, even those very low in nature, have the ability to illicit adverse health effects. A study conducted in 2017 examined the short-term impact of air pollution on population mortality. The researchers established a method to match and compare attributable deaths between individuals exposed to pollution levels exceeding 40 µg/m^3

and individuals exposed to pollution levels lower than 40 μg/m^3 (Baccini, Mattei, Mealli, Bertazzi, & Carugno, 2017). They found that exposures greater than 40 μg/m^3 were associated with 1079 deaths (CI = 116, 2042) with elderly individuals impacted the greatest accounting for 797 deaths from cardiovascular related disease and 243 deaths from respiratory related disease (Baccini et al., 2017).

There have been several major cases where breathing contaminated air in the workplace has led to chronic health issues. Mesothelioma, silicosis, black lung, and tuberculosis are examples of specific diseases that have impacted workers that breathed contaminated air in their workplace. The National Institute for Occupational Safety and Health (NIOSH) has conducted research into these and other pulmonary diseases to define how the different causative agents behave, how they illicit their harmful effects, and how they can be eliminated or controlled. In response to data collected during research activities, the Occupational Safety and Health Administration has passed regulations aimed at protecting workers exposed to different airborne contaminants (Occupational Safety and Health Administration, 1995, 2017).

While aerosol research studies can use specific agents known to cause disease, this one will not. Rather, one of the aims of this study was to aerosolize fluorescent polystyrene latex spheres (FPLSs) to validate a wind tunnel performance. These polymer spheres are available in a variety of sizes similar to those of specific harmful agents making them ideal for aerosol research. The FPLSs that were used can be seen in Figure 1: 0.5 μm and 2.0 μm FPLS Liquid Suspensions (Pictured Left) 6.0 μm and 12.0 μm FPLS Dry Powders (Picture Right). Using these spheres have two major advantages. The first advantage is that when ordered from the manufacturer, they are uniform in size

and shape. This allows the researcher to create a monodisperse aerosol for evaluation in a chamber or other testing environment. The following figures show the four test sizes of FPLS used in this study: Figure 2 - 0.5 µm FPLS under Phase Contrast and Fluorescence Microscopy, Figure 3 - 2.0 µm FPLS under Phase Contrast and Fluorescence Microscopy, Figure 4 - 6.0 µm FPLS under Phase Contrast and Fluorescence Microscopy, and Figure 5 - 12.0 µm FPLS under Phase Contrast and Fluorescence Microscopy. One can see that the FPLS are perfectly spherical and of the same size.

Figure 1: 0.5 µm and 2.0 µm FPLS Liquid Suspensions (Pictured Left) 6.0 µm and 12.0 µm FPLS Dry Powders (Picture Right).

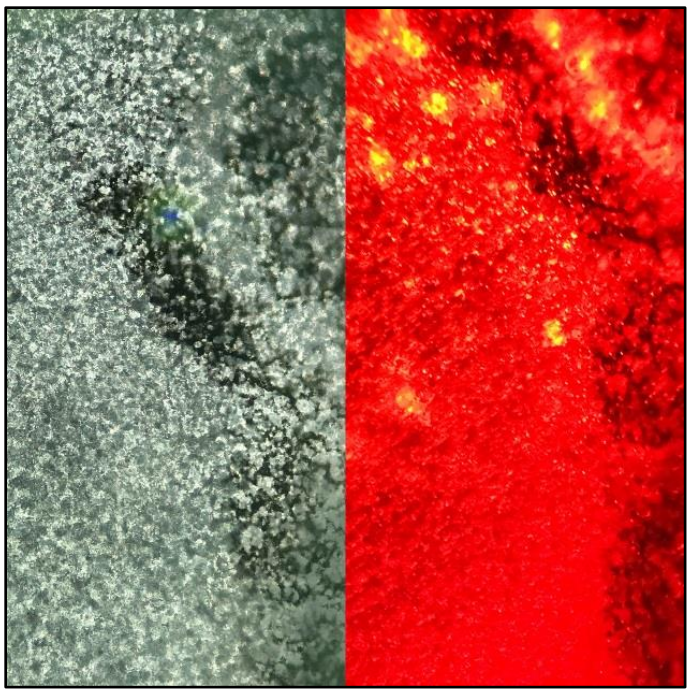

Figure 2: 0.5 µm FPLS under Phase Contrast and Fluorescence Microscopy.

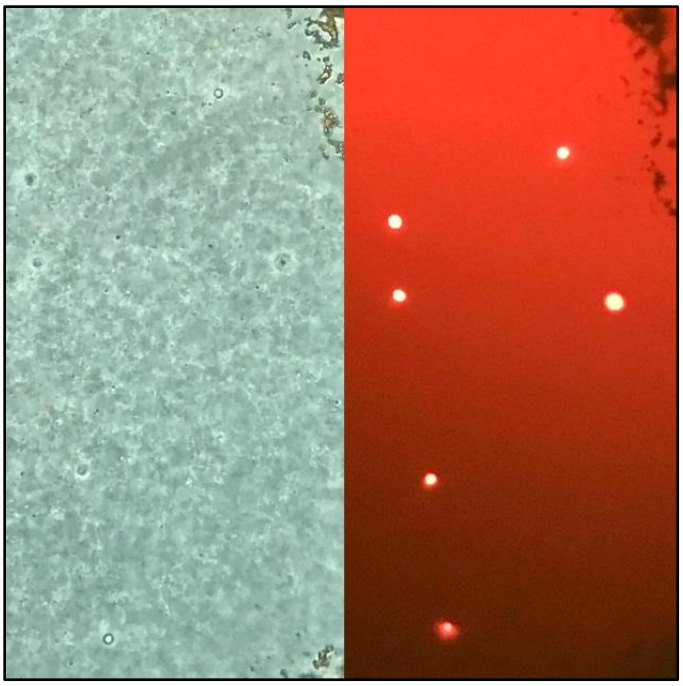

Figure 3: 2.0 µm FPLS under Phase Contrast and Fluorescence Microscopy.

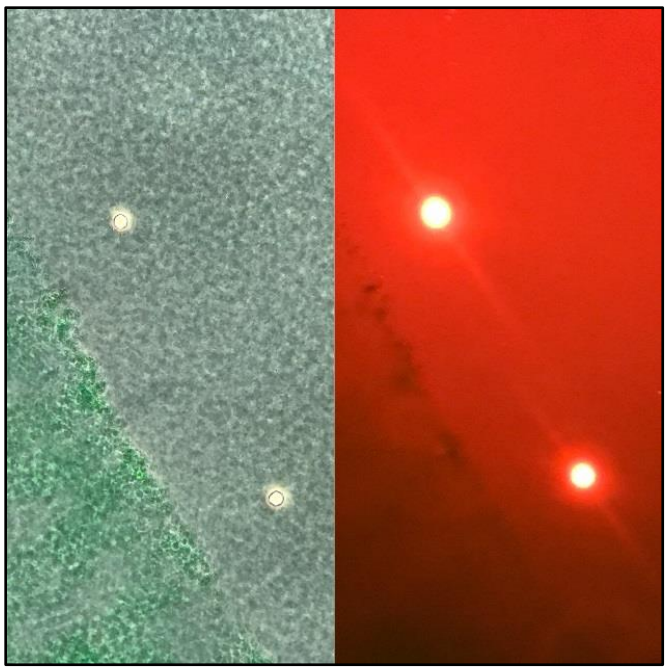

Figure 4: 6.0 µm FPLS under Phase Contrast and Fluorescence Microscopy.

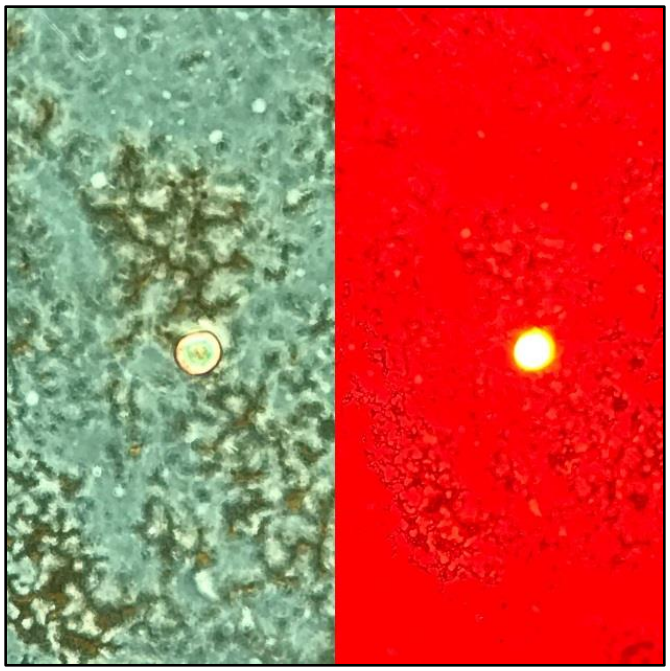

Figure 5: 12.0 µm FPLS under Phase Contrast and Fluorescence Microscopy.

The second major advantage is that these FPLS are marked with a fluorescent dye. During fluorometric analysis, only the particles of interest will by identified due to their fluorescent marker. Any other particles that are present in the testing environment will not be detected by the fluorometer and therefore not considered in analysis. FPLS have been successfully used in several industrial hygiene research studies making their use in this study consistent with the scientific literature (B. T. Chen, Feather, Maynard, & Rao, 2004; Lindsley, Schmechel, & Chen, 2006; Su, Tolchinsky, Chen, Sigaev, & Cheng, 2012). Since fluorescent polystyrene latex spheres come in liquid suspensions and dry powders depending on size, different aerosol generators were used to introduce particles into the testing environment.

Aerosol Generation from Liquid Suspensions

The most common aerosol generator for liquids or suspensions is the Collison Nebulizer. Early investigation with regard to the performance and application of this aerosol generator was described in the 1970's (May, 1973). Individuals conducting aerosol research find this generator quite useful as it has the ability to generate reasonably uniform droplets with a mass median diameter of 2 µm. Droplets and particles of 2 µm or less are of particular interest due to their propensity to deposit deep in the pulmonary tract. The Collison Nebulizer is operated by using a compressed gas to draw a liquid or suspension into a jet (BGI Inc, 2002). The movement through the jet cuts the liquid or suspension where it forms into droplets (BGI Inc, 2002). These droplets are then forced out of the nozzle causing larger droplets to impact against the side of the glass jar (BGI Inc, 2002). Smaller droplets are carried out of the jar by air into the testing

environment (BGI Inc, 2002). Depending on the scientific application and required output, there are one, three, six, and twenty-four jet models.

Because this research experiment required utilization of large air flow rates in the wind tunnel, several Collison Nebulizers would have been required to reach appropriate aerosol concentrations in the wind tunnel. The use of several nebulizers would have been quite costly resulting in the need for a single aerosol generator capable of producing a high quantity of FPLS monodisperse aerosol concentrations. The Blaustein Atomizer (BLAM), manufactured by CH Technologies, is a relatively new aerosol generator that builds on the technology used in the Collison Nebulizer. It has the capability to produce particle diameters from approximately 0.2 µm to 2.5 µm at air flow rates ranging from 1.0 L/min to 6.5 L/min, liquid feed rates from 0.1 ml/min to 1 ml/min, and air pressures from 5 psig to 90 psig (CH Technologies). Very few studies exist that have used this instrument making its use in this study quite valuable. The BLAM aerosol generator can be seen in Figure 6.

Zhen et al conducted a systematic comparison of four different bioaerosol generators (Zhen, Han, Fennell, & Mainelis, 2014). More specifically, the Collison Nebulizer, the BLAM, the C-Flow Nebulizer, and the Liquid Sparging Nebulizer were used to quantify culturability and cell membrane integrity when aerosolizing *Escherichia coli*. The researchers found that at particle output concentrations of ~100 particles/cm^3, the BLAM preserved the culturability of *E. coli* when compared to the three other generators at a $p<0.05$ (Zhen et al., 2014). At particle output concentrations of ~1000 particles/cm^3, the BLAM also showed a low cell membrane damage index when compared to the Collison Nebulizer at $p<0.001$ (Zhen et al., 2014).

A master's thesis by Bowling (2016) compared the Collison Nebulizer with the BLAM. In separate experiments, *Francisella tularensis,* Influenza, and Rift Valley Fever Virus were introduced into a nose-only tower using the different nebulizers (Bowling, 2016). The researcher found that the Collison had a better spray factor, aerosol efficiency, and organism viability when compared to the BLAM (Bowling, 2016). It should be noted that the BLAM was run in multi-pass mode for this research study unlike the single pass mode used in the study referenced above. It should also be noted that the BLAM used FPLS in this study rather than the biological agents used in the referenced study. It is possible for the performance characteristics to differ significantly based on these two changes.

Figure 6: The BLAM Aerosol Generator.

Atomization occurs in the BLAM when compressed air enters the stem on the main body and passes through eight jets at the speed of sound. (CH Technologies; Reed, Xhillari, Weiss, & Jaeger, 2016) The result is a vacuum in the space between the jet plate and the expansion plate which forces the liquid from the well to the individual jets (CH Technologies; Reed et al., 2016). Once the liquid reaches the area around the jets, it is formed into small droplets and is sprayed down where it impacts on the liquid contained inside the collection jar (CH Technologies; Reed et al., 2016). After impaction, the smaller particles make a 180° turn and are forced out of the atomizer and into the testing environment. Because of inertial forces, larger particles will be unable to make the turn and will impact on the liquid surface while smaller particles will remain suspended in the airstream where they exit the atomizer. (CH Technologies; Reed et al., 2016) One unique function of this aerosol generator is that it offers both single pass operation, multi-pass operation and multi-pass operation with external refill. In single pass mode, the test liquid is fed externally by a syringe or peristaltic pump until it is exhausted while in multi-pass mode the test liquid is preplaced in the atomizer jar and recirculated until it is depleted (CH Technologies; Reed et al., 2016). For this research study, the BLAM was run in multi-pass mode so that it used red fluorescent polystyrene latex sphere suspensions of 0.5 µm and 2.0 µm efficiently.

Aerosol Generation from Dry Powder

Depending on product availability and specific application, a liquid aerosol generator may not always be a practical choice. Instead a dry powder aerosol generator may be needed. Dry particle aerosol generators typically have two major requirements: (1) they must have a way to continuously introduce powder into the generator at a

constant rate and (2) they must have a way to turn the powder into an aerosol (National Research Council, 2006). Several models of dry powder aerosol generators are available on the market today and may use fluidized beds, fluid energy jet mills, or venturi tubes to aerosolize and disperse dry powders (B. Chen, Yeh, & Fan, 1995). One of the most popular being the Wright Dust Feeder, which has been used in many different research studies (Pieretti, 2010; Riley, 2016; Yi et al., 2013)

The Vilnius Aerosol Generator (VAG), manufactured by CH Technologies, is a relatively new instrument used to produce aerosols from dry powder. It has the capability to produce particles, ranging from 5.0 µm to 12.0 µm, at concentrations from 0 to 160 g/m^3 (CH Technologies, 2016). Air flow rates required for generation range from 6.0 L/min to 13.0 L/min with generation lasting up to six hours. The VAG Aerosol Generator can be seen in Figure 7. As with the BLAM, very few studies exist that have used this instrument making its use in this study quite valuable.

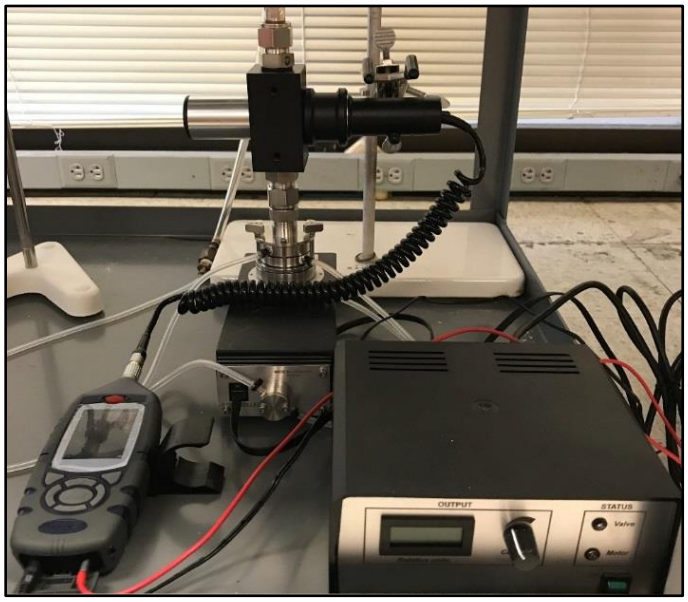

Figure 7: VAG Aerosol Generator.

In a 2009 study, pharmaceutical researchers developed a method to assess particle reentrainment and a possible stage coating for the Next Generation Pharmaceutical Impactor (J. Rissler, Asking, & Dreyer, 2009). The researchers selected the VAG to generate micronized insulin from dry powder for three reasons (1) they needed an aerosol generation system capable of efficiently dispersing pharmaceutical powders in the micron size range, (2) they needed an aerosol generation system that was able to produce consistent aerodynamic particle size distribution throughout experimentation runs, and (3) they needed an aerosol generation system that was able to produce a stable aerodynamic particle size distribution independent of sampling flow rate to the impactor (J. Rissler et al., 2009). The VAG successfully delivered 0.2 mg/s of micronized insulin per run and allowed the researchers to determine that an aqueous coating could successfully reduce particle reentrainment in the Next Generation Impactor (J. Rissler et al., 2009).

Two studies conducted in 2013 used the VAG to aerosolize lunar dust that was collected during the Apollo 14 space mission. In the first study, the VAG was used to assess the toxicity of lunar dust in inhalation-exposed rats (Lam et al., 2013). Fisher 344 rats, placed in restraint tubes, were exposed to lunar dust concentrations of 0, 2.0 to 2.5 mg/m^3, or 6.0 to 7.5 mg/m^3 for six hours (Lam et al., 2013). Biomarkers were used to assess toxic effects with the researchers finding pulmonary inflammation, septal thickening, fibrosis, and granulomas when rats were exposed to elevated concentrations (Lam et al., 2013). In addition, rats revealed that 6.8 mg/m^3 was the maximum no observable adverse effect level (NOAEL) (Lam et al., 2013).

In the second 2013 study, the VAG was used to estimate safe human exposure levels for lunar dust (Scully, Lam, & James, 2013). The VAG was used to generate lunar dust with mass median aerodynamic diameters of 2.5 µm (Scully et al., 2013). Fisher 344 rats were then exposed to this dust six hours a day, five days a week for four weeks (Scully et al., 2013). The researchers found that benchmark doses produced safe exposure estimate values ranging from 0.6 to 0.9 mg/m^3 (Scully et al., 2013)

Rissler et al (2017) conducted a study that examined deposition efficiency of inhaled particles related to breathing pattern and lung function. Particles from 15 to 5,000 nm were of particular interest with the study population being healthy children and adults (Jenny Rissler et al., 2017). The VAG was used to generate and disperse spherical glass particles from 500 to 5,000 nm with the researchers finding large variability between individuals (Jenny Rissler et al., 2017). The researchers believed that individual breathing pattern as well as individual lung anatomy and function may explain the variability (Jenny Rissler et al., 2017).

A final study that utilized the VAG for aerosol generation was a pharmacokinetic comparison between nebulized and dry powder INS1009, an inhaled lipid nanoparticle suspension, was used for rat exposure (Li et al., 2017). Liquid INS1009 was nebulized by the Aeroneb Pro, with pulmonary doses of 15.6 and 5.5 µg/kg and dry powder INS1009 was aerosolized by the VAG producing pulmonary doses of 5.7 and 2.0 µg/kg with both generators having mass median aerodynamic diameters ranging from 2.65 to 3.19 µm (Li et al., 2017). The researchers found that with the VAG, they could successfully aerosolize INS1009 from a dry powder to be used in nose-only inhalation studies. The scientific

articles discussed here illustrate that the VAG can consistently produce desired particle sizes from dry powder which made it acceptable for use in this study.

The way that the VAG aerosolizes dry powder is quite unique. The first unique feature is the dust chamber which houses a turbine. When the VAG is activated and compressed air runs through the system, the bottom membrane of the dust chamber vibrates and the turbine inside spins aerosolizing the dry powder placed inside (CH Technologies, 2016). Above the dust chamber is a deagglomeration assembly. The deagglomeration assembly contains jets that shoot air and break up agglomerated particles. This ensures that only single particles are delivered to a testing environment to be captured for analysis. The aerosolized particles leave the dust chamber and are pushed into the testing environment by compressed air. The second unique feature of the VAG is that it has a built in automatic feedback system. When the controller is set to produce a desired aerosol concentration, a built-in aerosol monitor ensures that this concentration is maintained throughout the testing period (CH Technologies, 2016). When the level drops below the set concentration, a valve opens on the VAG, rerouting air and allowing it to produce more particles. Once the concentration climbs back to its set point, the valve closes. These characteristics of the VAG made it a suitable choice as the dry powder aerosol generator. For this research study, the VAG was used to produce 6.0 µm and 12.0 µm monodisperse aerosol concentrations of red fluorescent polystyrene latex spheres from dry powder.

Wind Tunnel Use in Aerosol Research

Special instruments have been designed to help industrial hygienists quantify the amount of particulate exposure. Once exposures and their sources are identified, they

may be eliminated or a suitable control measure may be designed. Much of the laboratory research related to industrial hygiene instrumentation has been completed in environmental chambers. These special instruments can be placed in these chambers and exposed to an agent of interest allowing for the capture of information related to performance and efficiency. Chambers allow the researcher to control many of the variables that can influence project success including temperature, pressure, and humidity. While these studies offer valuable baseline data, they evaluate instruments under well controlled conditions and may not be representative of actual conditions faced in the occupational setting. Wind tunnels have been used for quite some time to evaluate industrial hygiene instrumentation and have the ability to simulate field conditions. By simulating field conditions, one may gain a better understanding of instrument performance in moving air conditions similar to real world situations.

A study conducted by Hinds and Kuo in 1998 used a wind tunnel to test inhalability and sampler performance following exposure to particles with larger mass median diameters. (William C. Hinds & Kuo, 1995) The wind tunnel was operated at wind speeds varying from 20 fpm to 390 fpm and had the ability to house a full torso mannequin inside for sampler evaluation. The researchers found that the wind tunnel could produce uniform velocity from 40 fpm to 390 fpm, had turbulence from 3% to 14%, had uniform aluminum oxide dust generation in the center region of the wind tunnel testing section, and had good performance for particles with aerodynamic diameters of 10 µm to 145 µm. (William C. Hinds & Kuo, 1995)

Wagner and Leith (2001) used a wind tunnel to examine the efficiency of passive aerosol samplers. (Wagner & Leith, 2001) They used a 2.4 m long rectangular duct that

introduced aerosols on one end and pulled air through the other. Inside the duct, incoming air encountered an aerosol cloud created by a nebulizer, turbulence screens, an optical particle monitor, an anemometer, passive samplers, and an impactor plus an isokinetic probe. For experimentation, the wind tunnel was run at speeds ranging from 1.5 to 5 m/s. The researchers were able to successfully deliver high concentrations of polydisperse, nonvolatile dust in this wind tunnel with aerosol concentrations having a CV of <6% inside the wind tunnel testing section and the passive samplers having a $CV_{PM2.5}$ = 18.1% and CV_{PM10} = 32.2%. (Wagner & Leith, 2001)

A study conducted in 2008 used an ultra-low speed wind tunnel to examine personal sampler performance at wind speeds from 0.1 to 0.5 m/s. (Schmees, Wu, & Vincent, 2008) Alumina powder particles with aerodynamic diameters ranging from 6 to 90 µm were of particular interest and were introduced into a newly designed wind tunnel complete with a life size mannequin in the testing section. The mannequin used in the study was able to breath on its own and was capable of being heated to human body temperature. This allowed the researchers to simulate how normal human respiration impacted aerosol behavior near the personal samplers. They found through flow visualization that air exiting the respiratory tract may have an impact on the distribution of particles in or near the breathing zone. The researchers explained that further study using the newly designed wind tunnel will focus on personal sampler aspiration efficiency relative to breathing zone of the life-like mannequin. (Schmees et al., 2008) For this study, a wind tunnel was designed, constructed and characterized to be used for industrial hygiene research.

Isokinetic Sampling

An isokinetic sampler is the main method that will be used to characterize the capabilities of the wind tunnel. Sampling isokinetically with a specially designed probe will guarantee that a representative sample of fluorescent polystyrene latex spheres enter the inlet of the probe at the same velocity as the air moving through the wind tunnel (William C Hinds, 1999). These wind characterization methods are well described in the scientific literature (Lee, Yu, & Kim, 2013; Su et al., 2012; Wagner & Leith, 2001). Superisokinetic sampling will occur if the velocity entering the probe is greater than the wind tunnel velocity and subisokinetic sampling will occur if the wind tunnel velocity is greater than the velocity of the probe (William C Hinds, 1999). Proper alignment of the probe in the tunnel is critical because superisokinetic or subisokinetic sampling will overestimate or underestimate the true aerosol concentration in the wind tunnel.

Specific Aims

The goal of this project was to design, construct, and characterize a wind tunnel to be used for aerosol research. Design and construction of the various wind tunnel components were performed according to the information found in the scientific literature on wind tunnels. Following reported best practices ensured that the wind tunnel operated within established parameters allowing researchers to produce reproducible and reliable data. Characterization using the BLAM and VAG aerosol generators contributed to the scientific body of knowledge as neither had been used in this type of application. Both were used to demonstrate that monodisperse aerosols of sizes that are related to human health could be introduced into the designed and constructed wind tunnel, collected by an isokinetic sampler, and detected using fluorometry. Once the wind tunnel was characterized and the results were deemed acceptable, it will be ready for use in future aerosol research experiments focused on particle behavior in moving air.

Aim 1: To design a wind tunnel based on best practice information outlined in scientific literature.

Wind tunnel filter housings, settling chamber, contraction section, testing section, diffuser, and fan were carefully designed to ensure that they created flow patterns inside the wind tunnel that were appropriate for the introduction and collection of aerosols. The goals of this aim were to:

A. Use HEPA filters installed in housings capable of removing 99.97% of particulate matter in air entering and exiting the wind tunnel to ensure a clean working environment.
B. Design a settling chamber that reduces air turbulence by using honeycomb flow straighteners with openings 8-10 times greater than their length and two sets of screens with open air ratios greater than 0.57.
C. Design a contraction that further reduces air turbulence entering the testing section by using an entrance and exit ratio between 4 and 9.
D. Design a testing section that can accommodate the introduction of monodisperse aerosols, the mixing of monodisperse aerosols in moving air, and collection of aerosols moving through the testing section.
E. Design a diffuser that has an angle less than 5 degrees to reduce the development of turbulence in the air stream.
F. Select and use a fan capable of moving the air through the wind tunnel at wind velocities up to 2.0 m/s.

Aim 2: To construct an operable wind tunnel to be used for aerosol research.

The construction of each component of the wind tunnel was completed according to design specifications. Failure to do so had the potential to introduce turbulence into air moving through the testing section thereby impacting the proper collection of introduced aerosols. The goals of this aim were to:

A. Identify a company that could construct filtering housings according to design specifications.
B. Identify a carpenter that could construct the settling chamber, contraction, and diffuser according to design specifications.
C. Identify a plastic fabrication company that could construct the testing section according to design specifications.
D. Identify a company that could supply a fan according to design specifications.

Aim 3: To characterize wind tunnel performance by examining the wind tunnel velocity profile, turbulence intensity, and aerosol introduction/collection.

After the construction of each wind tunnel component, the wind tunnel was assembled. Once assembled, the wind tunnel's operation was tested to ensure validity of the design. Goals of this aim were to:

A. Determine if the wind tunnel velocity profile differed within +/- 10% in the 16 quadrants of a cross-section of the tunnel's testing section.
B. Determine if the wind tunnel turbulence intensity exceeded 10% in the 16 quadrants of a cross-section of the tunnel's testing section.
C. Determine if monodisperse aerosol concentrations of 0.5, 2.0, 6.0, and 12.0 µm could be introduced, collected, and detected using an isokinetic sampler at wind tunnel velocities of 0.5, 1.0, and 2.0 m/s.

Experimental Methods

Wind Tunnel

Wind tunnels are constructed in two configurations: open circuit and closed circuit. The open circuit wind tunnel allows air to move directly through the different wind tunnel components to the exhaust section while a closed circuit wind tunnel recycles air already contained in the duct work. (Barlow, Rae II, & Pope, 1999) The open circuit wind tunnel used in this study was designed by Dr. Yehia Hammad, Industrial Hygiene Professor in the College of Public Health at the University of South Florida, and Jason Garcia, a Doctoral Candidate in Industrial Hygiene at the University of South Florida. It is housed in the Breath Lab, part of NEC Building on the University's campus. The wind tunnel spans a total of 20 feet in length. The major components are a filter housing at the tunnel entrance, a settling chamber, a contraction, a testing section, a diffuser, a filter housing at the tunnel exit, a fan, and an exhaust duct. In addition, an aerosol generator and radioactive source were incorporated into the final design. The wind tunnel blueprint can be seen in Figure 8 and the wind tunnel schematic diagram in Figure 9.

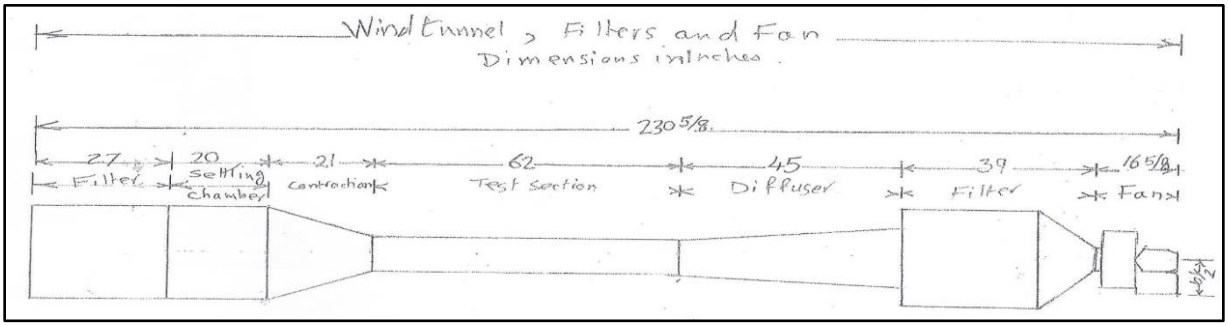

Figure 8: Wind Tunnel Blueprint.

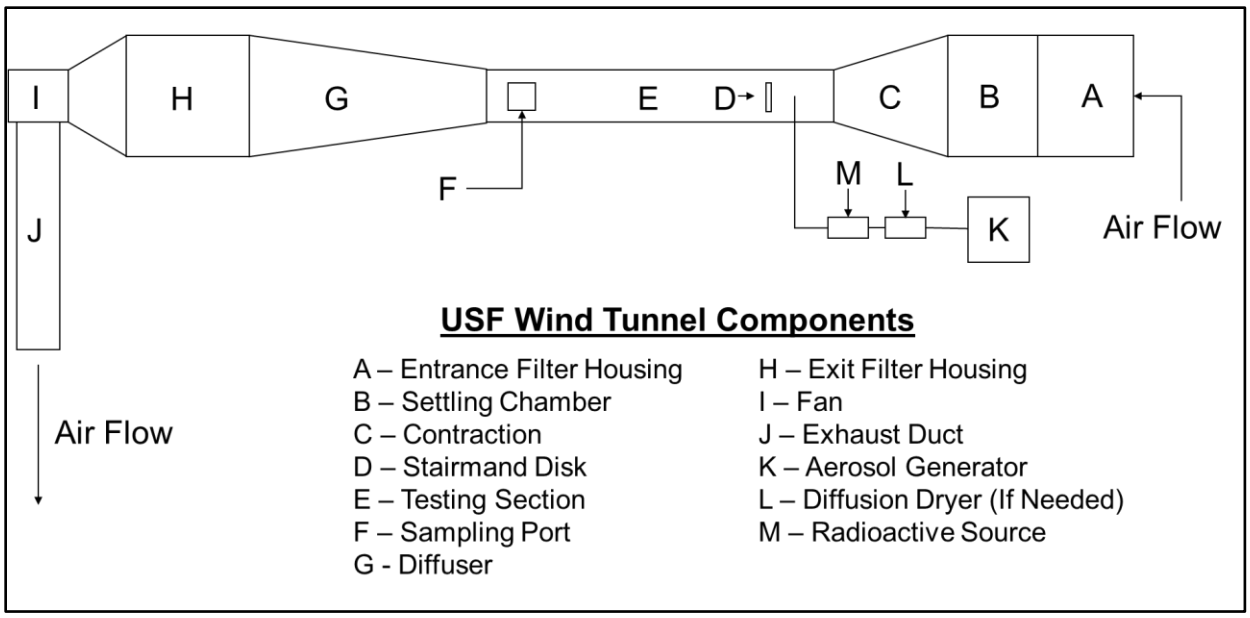

Figure 9: Wind Tunnel Schematic Diagram – Top View.

Each major component shown in the wind tunnel schematic diagram was acquired from an appropriate supplier. The filter housing at the entrance of the wind tunnel was specially designed and constructed by AAF International (Louisville, KY). The housing was designed to fit a 24 in. x 24 in. x 2 in. pre-filter, which removed particles greater than 1 µm in supply air, and a 24 in. x 24 in. x 11.5 in. HEPA filter, which removed 99.97% of 0.3 µm particles in supply air. The purpose of the filters at the entrance of the wind tunnel was to ensure that supply air entering the wind tunnel is free of particulate matter and that only the test aerosol is introduced in the testing section. The filter housing was constructed of 12 and 14 gauge galvanized steel with joints welded and sealed with an RTV sealant. Magnahelic pressure gauges were attached to the filter housing to measure the pressure drop across the filters. The entrance filter housing had a custom transition with 1.5 in. horizontal and 1.5 in. vertical flanges. These flanges were matched to flanges on the settling chamber. A neoprene gasket was placed between the flanges and were

secured together using bolts, lock washers, and nuts. The wind tunnel entrance filter housing can be seen in Figure 10.

Figure 10: Wind Tunnel Entrance Filter Housing.

The construction of the wind tunnel settling chamber, contraction, and diffuser were completed by Garden Carpentry, Inc. (Tampa, FL). The settling chamber, the contraction, and the diffuser were constructed out of 0.375 in. double sided pine wood. The interior of each wooden component was painted with static control epoxy coating. (The Sherwin Williams Company, 2015) The durable coating helped the wind tunnel withstand temperature and humidity fluctuations that are common in the Tampa Bay area.

The settling chamber of the wind tunnel accepts incoming air from the filter housing and directs it towards the contraction. The outside dimensions of the settling chamber

are 24.375 in. x 24.375 in. x 20 in. with the inside dimensions being 24 in. x 24 in. x 20 in. A 1.25 in. flange surrounds the settling chamber and allows for it to be connected to the entrance of the contraction. The main purpose of the settling chamber is to reduce turbulence in the air flow resulting in a more uniform pattern. Literature related to wind tunnel design suggests that using honeycomb in combination with screens in a settling chamber can reduce air stream turbulence to acceptable levels. (Mehta and Bradshaw, 1979; Singh et. al, 2013; Kulkarni et. al, 2011) The outside of the wind tunnel settling chamber can be seen in Figure 11.

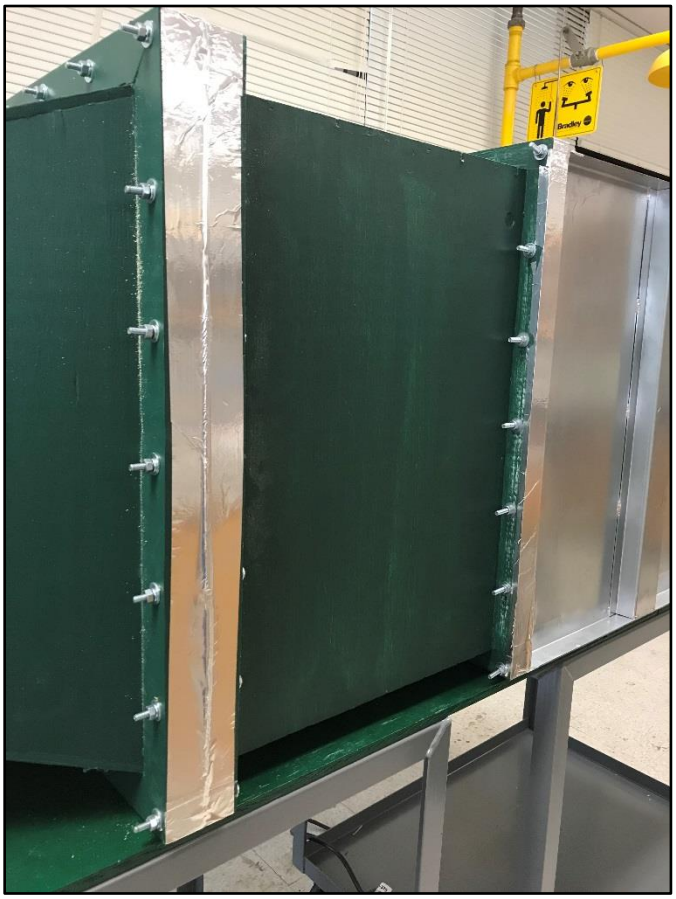

Figure 11: Outside of the Wind Tunnel Settling Chamber.

Honeycombs used in wind tunnel settling chambers typically have cells that are one of four different shapes: circular, square, hexagonal, or triangular. The honeycomb used for this wind tunnel were purchased from Flatiron Panel Products, LLC (Lafayette, CO) and were hexagonal with a length and height of 24 in. to fit inside the interior of the settling chamber. Scientific literature indicates that to ensure maximum reduction of turbulence, honeycomb depth should be approximately 8-10 times its diameter. (Kulkarni, Sahoo, & Chavan, 2011) In this case, the diameter of one individual hexagon cell was approximately 0.25 in. Therefore the honeycomb cell depth could range from 2.0 in. to 2.5 in. Based on product availability, the honeycomb used in this wind tunnel had a depth of approximately 2.5 in. making the overall size of the honeycomb 24 in. x 24 in. x 2.5 in. Honeycomb on the inside of the wind tunnel settling chamber can be seen in Figure 12 and a close up of honeycomb on the inside of the wind tunnel settling chamber can be seen in Figure 13.

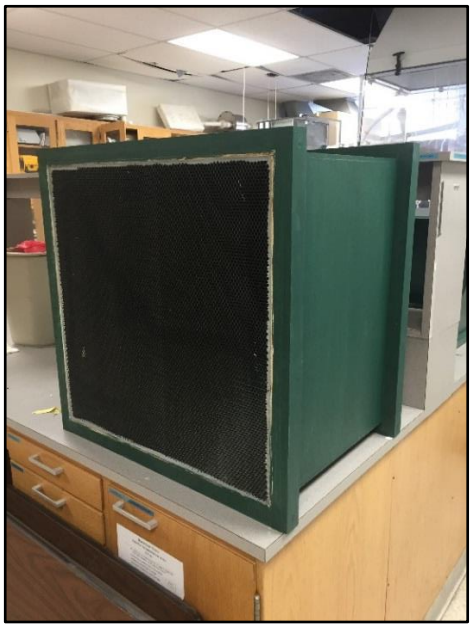

Figure 12: Inside of the Wind Tunnel Settling Chamber.

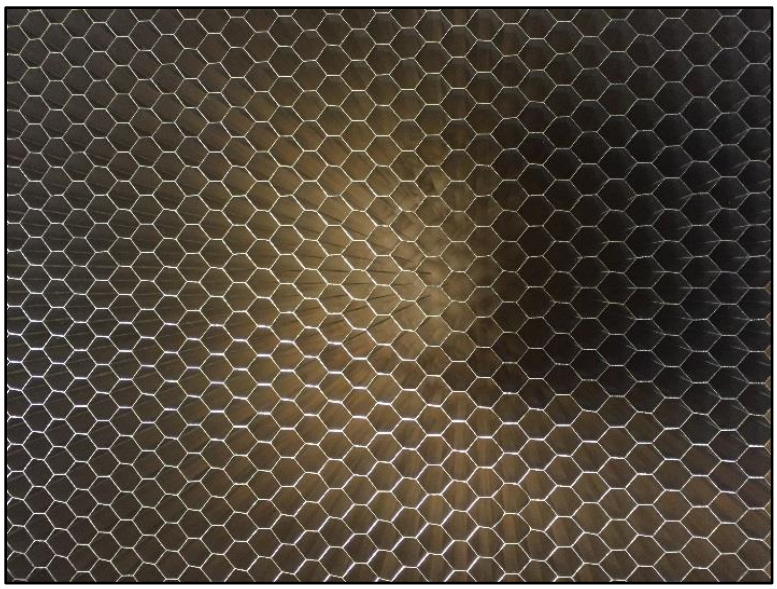

Figure 13: Close Up of Honeycomb on the Inside of the Wind Tunnel Settling Chamber.

Mesh screens are used after the honeycomb to further straighten airflow approaching the testing section in a wind tunnel. Wire type and diameter play an important role on how well it performs at reducing turbulence. Kulkarni et. al (2011) suggest that screens should have an open area ratio (β) that is greater than 0.57. Values greater than 0.57 help to diminish directional irregularities in the air stream. Screen open-area ratio is calculated using Equation 1:

$$\beta = (1 - \frac{d_s}{L_s})^2 \qquad \text{(Equation 1)}$$

Where β is the open-area ratio, d_s is the screen wire diameter and L_s the screen length. (Singh, 2013) The open-area ratio of the screen used in our wind tunnel was calculated to be 0.99, which was greater than 0.57 parameter stated in the literature and therefore was acceptable. Wire screens were used rather than other types due to ready availability. The mesh screen on the inside of the wind tunnel settling chamber can be seen in Figure 14.

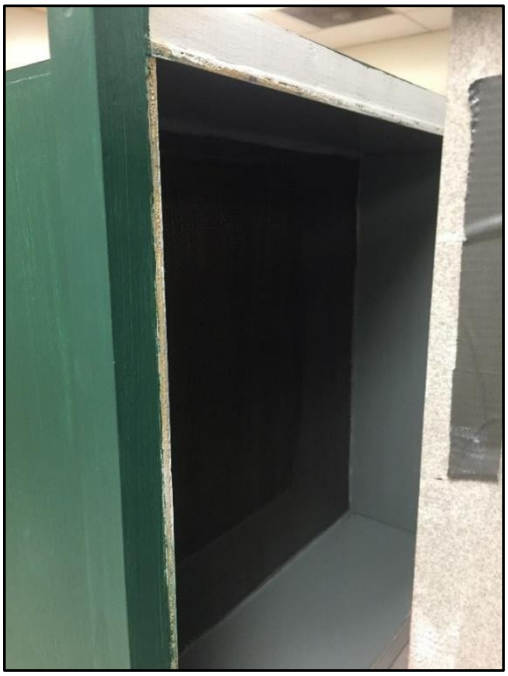

Figure 14: Mesh Screen on the Inside of the Wind Tunnel Settling Chamber.

The shape of honeycomb and the number of screens used in wind tunnel settling chambers has been the topic of several different research studies. Kulkarni et. al (2011) conducted a simulation of honeycomb-screen combinations to reduce turbulence in a subsonic wind tunnel. The researchers found that using honeycomb alone will not provide significant turbulence reduction in wind tunnel settling chambers and the use of screens in conjunction with honeycomb is encouraged. In another study, researchers found that honeycomb combined with two screens provided the most turbulence reduction. (Scheiman & Brooks, 1981). Based on these results, the optimum reduction in turbulence was achieved using a honeycomb and two sets of screens installed into this wind tunnel settling chamber.

One important feature of the honeycomb and screens used to straighten air flow in the wind tunnel settling chamber is their spacing. Mehta and Bradshaw (1979) stated

that honeycomb and screens should be 0.2 duct diameters apart from one another to ensure proper performance. In order to determine the correct spacing for these flow straighteners, the hydraulic duct diameter of the settling chamber must be calculated since a non-circular settling chamber is used. The hydraulic duct diameter is calculated using the following Equation 2:

$$D_h = \frac{4WH}{2(W+H)} \qquad \text{(Equation 2)}$$

where D_h is the hydraulic duct diameter, W is the duct width, and H is the duct height. For our application, the chamber width and height will be 24 in. Inserting 24 in. for width and 24 in. for height in the equation detailed above, the hydraulic duct diameter was calculated to be 24 in. For this application, that would be approximately 4.8 in. apart. For ease in construction, this value was rounded up to 5 in. Therefore there was 5 in. in between the honeycomb and the first screen as well as 5 in. in between the first screen and the second screen. The exit to the wind tunnel settling chamber was connected to the entrance of the wind tunnel contraction. A gasket was placed between the flanges of the settling chamber exit and the contraction entrance so that an airtight seal was achieved. The flanges were secured together using bolts, lock washers, and nuts.

The contraction section of a wind tunnel, seen in Figure 15, directs straightened air exiting the settling chamber into the testing section. The contraction reduces mean and fluctuating velocity variations to a smaller proportion of the average velocity while increasing the resultant mean velocity. (Abdelhamed, Yassen, & ElSakka, 2015) The total length of this wind tunnel contraction was 21 in. with the entrance of the contraction measuring 24 in. x 24 in. and the exit measuring 10.25 in. x 10.25 in. A study conducted in 2013 showed that larger contraction ratios combined with shorter contraction lengths

reduce power loss with optimal contraction ratios being between 4 and 9. (Singh, 2013) This wind tunnel had a contraction ratio of 5.5, well within the optimal performance range described in the literature. The entrance to the contraction has a 1.25 in. flange surrounding the opening and was connected to the exit of the settling chamber. The exit to the contraction has a 1.625 in. flange surrounding the opening and was connected to the testing section. A gasket was placed between the flanges of the settling chamber exit and the opening of the contraction. A gasket was also be placed between the flanges of the contraction exit and the testing section entrance so that an airtight seal was achieved. The flanges were secured using bolts, lock washers, and nuts.

Figure 15: Wind Tunnel Contraction.

The construction of the wind tunnel testing section was completed by B & R Sales (Clearwater, FL). The testing section was constructed of 0.5 in. acrylic plastic with an overall length of 62 in. and an interior height and width of 10.25 in. The entrance of the testing section was built with a 1.5 in. flange to allow it to be connected to the contraction. The exit of the testing section was also built with a 1.5 in. flange to allow it to be connected to the diffuser. Neoprene gaskets were placed between both sets of flanges and they were secured using bolts, lock washers, and nuts. In addition, clamps were placed at the four corners of the entrance and exit flange of the testing section to ensure an air tight seal. The wind tunnel testing section can be seen in Figure 16.

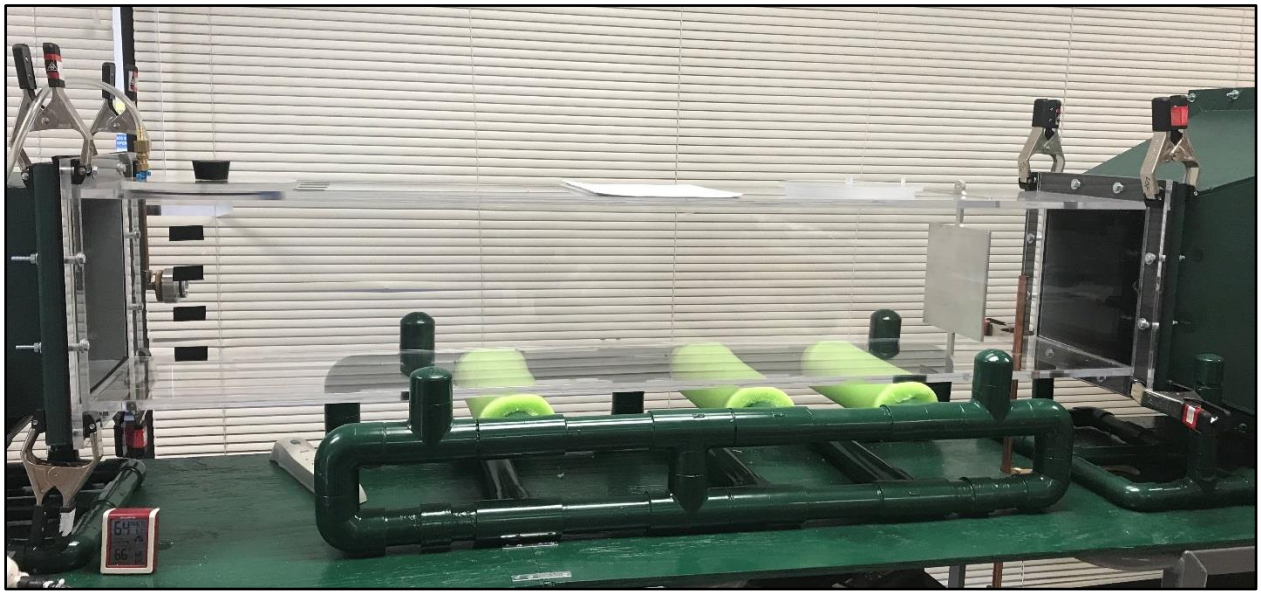

Figure 16: Wind Tunnel Testing Section.

A 0.625 in. hole was drilled in the center of the bottom acrylic panel, approximately 5.125 in. from the entrance of the testing section. The purpose of this hole was to accommodate a 0.625 in. copper pipe to be used for delivering test aerosols into the wind

tunnel testing section. The inserted copper pipe extended approximately 5.125 in. into the interior of the wind tunnel. This horizontally and vertically centered delivery of test aerosols in the middle region of the testing section. Air moving through the testing section encountered a specific size aerosol cloud, mixed with it, and delivered it towards sampling instruments at the opposite end of the wind tunnel. The specific method used to generate test aerosols is discussed in a later section. The aerosol introduction pipe in the wind tunnel testing section can be seen in Figure 17.

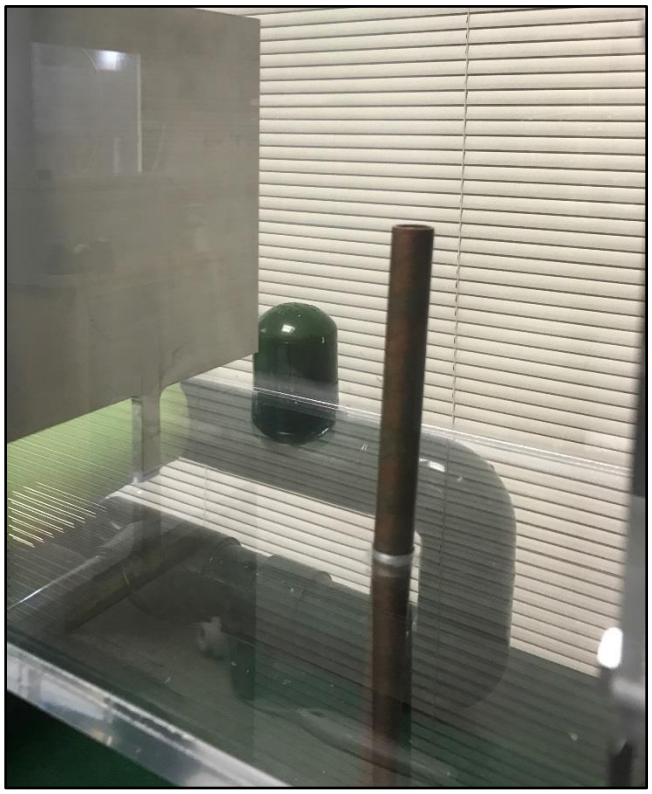

Figure 17: Aerosol Introduction Pipe in the Wind Tunnel Testing Section.

As previously discussed, air entering the testing section of the wind tunnel was HEPA filtered. Any air traveling through the wind tunnel after the entrance filter housing

contained only test aerosols used for experimentation. Monodisperse test aerosol entering the wind tunnel through the copper pipe in the testing section mixed with incoming air to allow for transport through the wind tunnel. In this wind tunnel, a Stairmand disk was used to mix test aerosols into the moving air stream. A Stairmand disk is a same shape as the duct used to transport air. It purposely blocks air in the middle region of the air duct creating eddies resulting in turbulent air on the upstream side. This turbulent air pattern is used to mix the test aerosols that are delivered immediately before the disk. Once mixed, the test aerosol moves around the disk and continues through the wind tunnel towards the test instruments. The use of this type of aerosol mixing device was originally described in 1941 and had been used in several applications since then. (Stairmand, 1941; Ramachandran, Sreenath, & Vincent, 1998; Su et al., 2012)

In order to create the proper amount of turbulent air on the upstream side of the disk and laminar air on the downstream side of the disk, it had to be a specific size in relation to the duct where it was placed. As previously explained, the hydraulic duct diameter had to be calculated since a rectangular duct was being used rather than a circular duct. Equation 1 can be used to determine the hydraulic duct diameter. For this testing section, the duct width and height were both 10.25 in. Inserting the 10.25 in. for width and 10.25 in. for height in the formula detailed above, the hydraulic duct diameter was calculated to be 10.25 in. In order to determine the size of the Stairmand Disk needed, the following formula was used:

$$SD = \frac{D_h}{\sqrt{2}} \qquad \text{(Equation 3)}$$

where SD is the Stairmand Disk size and D_h is the hydraulic duct diameter. (Air Techniques International, 2016) Inserting in 10.25 in. for the hydraulic duct diameter and dividing by the square root of 2, it was determined that the Stairmand disk for this wind tunnel testing section was required to be 7.25 in. in width and 7.25 in. in height.

The construction of the Stairmand Disk was completed by B & R Sales (Clearwater, FL). The disk was made out of 7.25 in. by 7.25 in. aluminum plate. A slot was cut in the top panel of the testing section so that the Stairmand disk can be inserted and removed as desired. The disk was placed 10.25 in. from the entrance of the testing section with 5.125 in. between the disk and the aerosol delivery pipe previously discussed. Based on scientific experience, the location of test samplers downstream from the Stairmand Disk were to be at a certain distance to ensure that turbulent air moving around the disk was given adequate time to transition into a more uniform flow pattern. The United States Department of Energy found that a distance of four to six duct diameters was necessary for turbulence to settle. (United States Department of Energy, 2003) For this duct, that meant that the test samplers could be 41 in. to 61.5 in. from the Stairmand Disk to ensure a more uniform flow. The Stairmand Disk in this wind tunnel was constructed to be at a distance of approximately 46.125 in. from the test instruments, well within the range described in the literature. It should be noted that during experimentation with this wind tunnel the Stairmand Disk was always in place as it was needed for aerosol mixing. The Stairmand Disk in the wind tunnel testing section can be seen in Figure 18.

Figure 18: Stairmand Disk in the Wind Tunnel Testing Section.

The diffuser of a wind tunnel, seen in Figure 19, directs air exiting the testing section into the downstream filter housing. The total length of this wind tunnel diffuser was 45 in. with the opening of the diffuser constructed at 10.25 in. x 10.25 in. and the exit of the diffuser constructed at 15 in. x 15 in. These dimensions were selected so that the angle from the diffuser entrance to the exit remained small, calculated at 3 degrees. Angles less than 5 degrees allow for stable air pressure increases and air velocity decreases while diffusers with angles larger than 5 degrees may experience boundary layer separation and turbulence. (Singh, 2013) The entrance to the diffuser has a 1.625 in. flange surrounding the opening and was connected to the test section. The exit to the diffuser has a 5.75 in. flange surrounding the opening and was connected to the downstream filter box. A gasket was placed between the flanges of the test section and the diffuser opening as well as between the flanges of the diffuser exit and the

downstream filter box so that an airtight seal was achieved. The flanges were secured together using bolts, lock washers, and nuts.

Figure 19: Wind Tunnel Diffuser.

The downstream filter housing, similar to the entrance filter housing previously discussed, was specially designed and constructed by AAF International (Louisville, KY). The filter box houses a 24 in. x 24 in. x 2 in. pre-filter and a 24 in. x 24 in. x 11.5 in. HEPA filter. Filters were placed at the exit of the wind tunnel to remove the test aerosol from the air stream. This ensures that clean air is exhausted from the wind tunnel into the laboratory. The filter housing was made of 12 and 14 gauge galvanized steel with joints welded and sealed with sealant. Magnahelic pressure gauges were attached to the filter housing to measure the pressure drop across the filters. The entrance side of the exit filter housing has a custom transition with 2.75 in. horizontal and 1.5 in. vertical flanges. These flanges were matched to flanges on the diffuser. A neoprene gasket was placed between the flanges and they were secured together using bolts, lock washers, and nuts.

The exit side of the filter housing has a custom transition that is circular with an inside diameter of 5.875 in. and an outside diameter of 8 in. This transition was matched to the flanges on the fan. A neoprene gasket was placed between the flanges and they were secured using bolts, lock washers, and nuts. The wind tunnel exit filter housing can be seen in Figure 20.

Figure 20: Wind Tunnel Exit Filter Housing.

The fan used to move air through the wind tunnel was purchased from The New York Blower Company (Willowbrook, IL). The fan is capable of moving air at 500 cfm at 6.23 in. wg., which was adequate for this research project. The specifics for the fan were as follows: Arrangement – 4, Dimensions – Size 106, Motor Mounting – 143T, Fan

Discharge – Clockwise Top Horizontal, Horsepower – 1.5, and Speed – 3600 RPM. (The New York Blower Company, 2013) The fan was activated by a digital controller. The entrance to the fan was made of steel and has an inside diameter of 5.875 in., outside diameter of 8 in., and a 2.125 in. flange. The flange at the fan exit was made of steel, has outside dimensions of 7.625 in. x 7.625 in., inside dimensions of 5.625 in. x 5.625 in., and a 2 in. flange. A custom exhaust duct, constructed out of insulated foam board, channeled air coming out of the fan into a laboratory hood. The wind tunnel digital controller can be seen in Figure 21, the wind tunnel fan, motor, and exhaust duct can be seen in Figure 22, and the University of South Florida Wind Tunnel can be seen in Figure 23.

Figure 21: Wind Tunnel Digital Controller.

Figure 22: Wind Tunnel Fan, Motor, and Exhaust Duct.

Figure 23: The University of South Florida Wind Tunnel.

Prior to conducting experiments with the wind tunnel, it was necessary to evaluate its performance to determine whether it was functioning properly. The first step was to determine the relationship between the digital controller frequency, measured in Hertz (Hz), and the velocity inside the testing section, measured in meters per second (m/s). Since the testing section can be run with the Stairmand disk present or absent, both configurations were examined. Velocity measurements were captured using the Testo Model 480 High End IAQ Measuring Instrument and the Degree of Turbulence Probe (Figure 24). The probe was inserted into the testing section of the wind tunnel using the specially designed lid made to accommodate the testing probe wand and isokinetic aerosol sampler (Figure 25). The probe was situated so that it was centered vertically and horizontally. Once situated, the fan and motor were activated and measurements were obtained from frequencies ranging from 1.0 Hz to 25.0 Hz. This information showed the relationship between digital controller setting and velocity inside the wind tunnel.

Figure 24: Testo Model 480 High End IAQ Measuring Instrument and the Degree of-Turbulence Probe.

Figure 25: Testo Model 480 High End IAQ Measuring Instrument and the Degree of Turbulence Probe inside the Wind Tunnel.

A velocity profile was also established for each of the wind speeds used in this experiment. In order to capture the velocity profile, a cross section of the testing section inside area was divided into 16 equal quadrants. The wind tunnel testing section measurement scheme can be seen in Figure 26. The Testo Degree of Turbulence Probe was inserted through the lid of the testing section and placed into the center of each quadrant. The probe was held in place with a laboratory stand and arm to ensure that the probe remained in position during measurement. Measurements of all 16 quadrants were taken using the Testo Model 480 High End IAQ Measuring Instrument and Degree of Turbulence Probe. Tests were completed 5 times for velocities of 0.5, 1.0, and 2.0 m/s. The mean, standard deviation, and coefficient of variation were determined from the measurements. For each velocity, there should not be a variance larger than +/- 10% (Lee et al., 2013; United States Environmental Protection Agency, 2016a). It should be noted that all velocity profile measurements were taken with the Stairmand Disk in place.

The Stairmand Disk is required for aerosol mixing so the wind tunnel was always run in this configuration.

Figure 26: Wind Tunnel Testing Section Measurement Scheme.

Once the fan controller settings and the velocity profiles were known for the different velocities, turbulence intensity measurements in the testing section of the wind tunnel were collected. A significant amount of effort went into designing the settling chamber to ensure that air entering the testing section was moving in a uniform fashion and turbulence intensity measurements verified adequate construction. The measurement scheme was the same as that for the velocity profiles and can be seen in Figure 26. The Testo Degree of Turbulence Probe was inserted through the lid of the testing section and placed into the center of each quadrant. The probe was held in place with a laboratory stand and arm to ensure that the probe remained in position during measurement. Measurements were taken in all 16 quadrants using the Testo Model 480

High End IAQ Measuring Instrument and Degree of Turbulence Probe. This was performed 5 separate times for velocities of 0.5, 1.0, and 2.0 m/s. The mean, standard deviation, and coefficient of variation were determined from the measurements. In terms of turbulence intensity, there are no established guidelines. Most researchers design to get the lowest possible value. Turbulent air may prevent test aerosols from reaching the test instruments or affect uniformity of concentrations, thereby skewing the results. One citation stated that turbulence levels lower than 10% in wind tunnel testing sections are considered satisfactory for research purposes. ("Boundary Conditions," 2003) It should be noted that all turbulence intensity measurements were taken with the Stairmand Disk in place. The Stairmand Disk is required for aerosol mixing so the wind tunnel was always run in this configuration.

Once the fan controller settings were determined, experimental runs were conducted at 0.5, 1.0, and 2.0 m/s. These velocities were selected as they are similar to those that could be encountered by workers in the occupational environment. A study conducted in 1998 surveyed indoor wind speeds and found that median wind speeds ranged from 0.05 to 0.4 m/s (Baldwin & Maynard, 1998). An additional study explained that indoor workers could experience wind velocities ranging from 0.1 to 1.0 m/s while those working outdoors may experience wind velocities greater than 1.0 m/s (Baron & John, 1999). Su et al. (2012) used a wind tunnel with speeds of 0.5, 1.0, and 2.0 m/s to test the performance of the NIOSH Two-Stage Bioaerosol Sampler. Based on a review of the literature, using wind velocities of 0.5, 1.0, and 2.0 m/s for this study was appropriate.

Aerosol Generation from Liquid Suspensions

Five experimental runs were conducted for both 0.5 µm and 2.0 µm particles at 0.5, 1.0, and 2.0 m/s. The FPLS dilution factor equation below was used to ensure that the suspension used was properly diluted to create single particles for collection (B. T. Chen, Fletcher, & Cheng, 2011; Raabe, 1968):

$$Y = \frac{F(d_v^3)e^{(4.5\ ln^2\ \sigma_g)}[1-0.5e^{(ln^2\sigma_g)}]}{(1-R)(d_p^3)} \qquad \text{(Equation 4)}$$

where Y is the dilution factor, R is the desired singlet ratio, and F is the volume fraction of single particles of diameter (d_p) in the original fluorescent polystyrene latex suspension. The volume median diameter and the geometric standard deviation of the droplet size distribution are represented by d_v and σ_g (B. T. Chen et al., 2011; Raabe, 1968). For the 0.5 µm FPLS, the variables were: F = 1% or 0.01, R = 95% or 0.95, d_p = 0.5 µm, d_v = 2.0 µm, and σ_g = 1.4. This gave a latex dilution factor of 9.38 for 0.5 µm FPLSs. For the 2.0 µm FPLS, the variables were: F = 1% or 0.01, R = 95% or 0.95, d_p = 2.0 µm, d_v = 2.0 µm, and σ_g = 1.4. This gave a latex dilution factor of 0.15 for 2.0 µm FPLSs.

The first step in setting up a test run using the BLAM was to activate the wind tunnel at the desired speed using the electronic controller wired to the wind tunnel motor and fan. The tunnel was allowed to run for five minutes prior to aerosol generation to ensure that air was moving through the system. During the wind tunnel warm up period, the aerosol generator was prepared for testing. To prepare the BLAM, the nebulizing head was detached from the solution jar and filled with 100 µl of the appropriate size fluorescent polystyrene latex sphere suspension and 100 ml of deionized water. The jar was then reattached back on to the nebulizing head. The inlet of the nebulizing head was connected to a compressed nitrogen gas line with Tygon tubing and the outlet was

connected to a diffusion dryer. The diffusion dryer, containing calcium sulfate and cobalt chloride, removed moisture from the airstream resulting in individual dry particles of desired size. A connection at the outlet of the diffusion dryer led to the inlet of a TSI Kr-85 Radioactive Source (Shoreview, MN) which was necessary to neutralize the electrostatic charges on the aerosol cloud. The outlet of the radioactive source was connected to the testing section of the wind tunnel where particles were introduced into the air stream. In order to generate particles with the BLAM, a calibrated compressed nitrogen tank regulator was set to 20 psi in order to generate a flow of approximately 7.1 L/min. The nitrogen gas flow was monitored using a TSI Model 4140 Mass Flow Meter (Shoreview, MN). The aerosol generation from liquid suspension setup can be seen in Figure 27.

Figure 27: Aerosol Generation from Liquid Suspension Setup.

To characterize the aerosol concentration produced by the BLAM inside the wind tunnel, a 1 inch isokinetic sampling probe was prepared for sampling. The body of the isokinetic sampling probe was unscrewed to reveal the base. SKC, Inc. (Eighty Four, PA) 5.0 µm pore size, 37 mm diameter PVC filters and backing pads were used for sampling. A filter and a backing pad were placed on the base. The body of the isokinetic sampling probe was then screwed back on to the base and it was connected to the testing section lid by a copper pipe. The copper pipe extended through a predrilled hole in the testing section lid. This allowed for the probe to be connected to the pipe inside the wind tunnel while a high flow sampling pump was attached to the other end of the pipe outside the tunnel. Based on the area of the isokinetic sampling probe and the selected velocities to be used in the wind tunnel, the flow rates for isokinetic sampling at 0.5, 1.0, and 2.0 m/s were 15.4, 30.9, and 61.7 L/min respectively. All connections were made using Tygon tubing and the flow rate through the probe was monitored using a TSI Mass Flow Meter (Model 4140). The 1 Inch isokinetic sampling probe disassembled can be seen in Figure 28, the 1 inch isokinetic sampling probe assembled can be seen in Figure 29, and the 1 inch isokinetic sampling probe suspended inside the wind tunnel testing section can be seen in Figure 30.

At the conclusion of a four hour sampling session, the wind tunnel and aerosol generator were stopped. The isokinetic sampling probe and its PVC filter were washed to determine the amount of FPLSs captured. The exposed filter was removed with tweezers and placed in a 50 ml polypropylene centrifuge tube. 10 ml of ethyl acetate was added to the centrifuge tube using a 10 ml pipet. With the tube capped, the liquid was gently shaken for 10 seconds to ensure that the walls of the centrifuge tube and filter are

coated with the solvent. The solution was allowed to sit for 20 minutes undisturbed before analysis. The inside walls of the isokinetic sampling probe were scraped with a rubber policeman to dislodge impacted particles. 10 ml of ethyl acetate was used to rinse the inside walls and the rubber policeman with the solution captured in a 50 ml polypropylene centrifuge tube. The solution was allowed to sit for 20 minutes undisturbed before analysis. Once the polystyrene latex spheres had an opportunity to dissolve and the fluorescein was in solution, the samples were analyzed using fluorometry.

Figure 28: 1 Inch Isokinetic Sampling Probe Disassembled.

Figure 29: 1 Inch Isokinetic Sampling Probe Assembled.

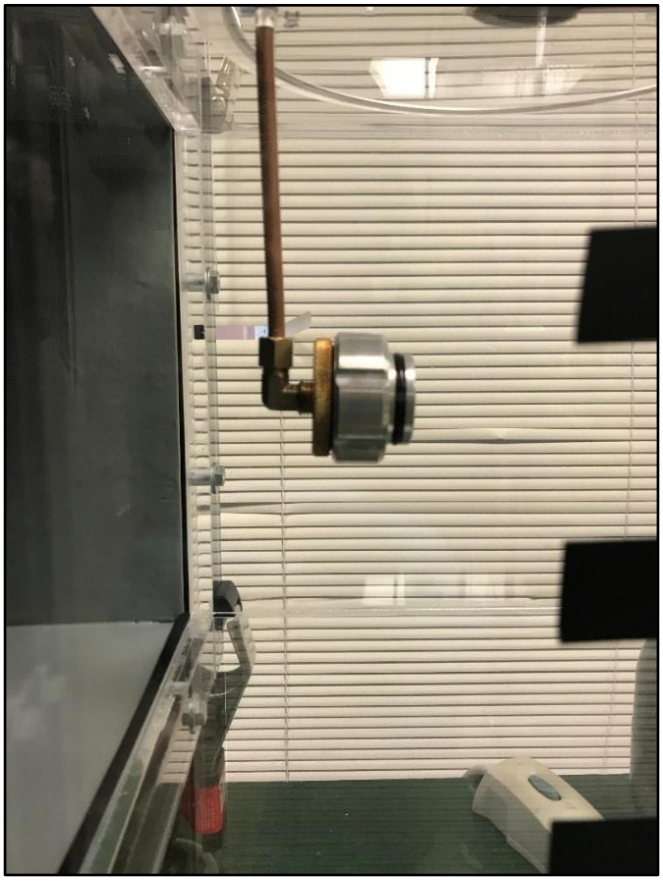

Figure 30: 1 Inch Isokinetic Sampling Probe Suspended Inside the Wind Tunnel Testing Section.

The Promega GloMax Jr. Fluorometer (Madison, WI), seen in Figure 31, was used for analysis. The unit used the Promega Part E6073 Green Filter (Madison, WI) to obtain maximum detection of the red fluorescent marker that was used to label the polystyrene latex spheres. The red fluorescent polystyrene latex sphere wavelength graph, used with permission, in Figure 32 shows these spheres have an excitation wavelength of 542 nm and an emission wavelength of 612. (Thermo Fisher Scientific, 2018). 190 µl of test solution was drawn up from the 50 ml centrifuge tube containing the PVC filter using a micropipette and was placed in a disposable glass mini-cell cuvette for measurement. 190 µl of test solution was drawn up from the 50 ml centrifuge tube that contained the rinse from the isokinetic sampling probe wall and rubber policeman. Duplicate samples were taken from each centrifuge tube. Each individual sample was read three times and the average fluorescent standard unit value was calculated. Using the red fluorescent polystyrene latex sphere calibration curve in Figure 33, the mass of FPLSs collected was determined.

Figure 31: Promega GloMax Jr. Fluorometer.

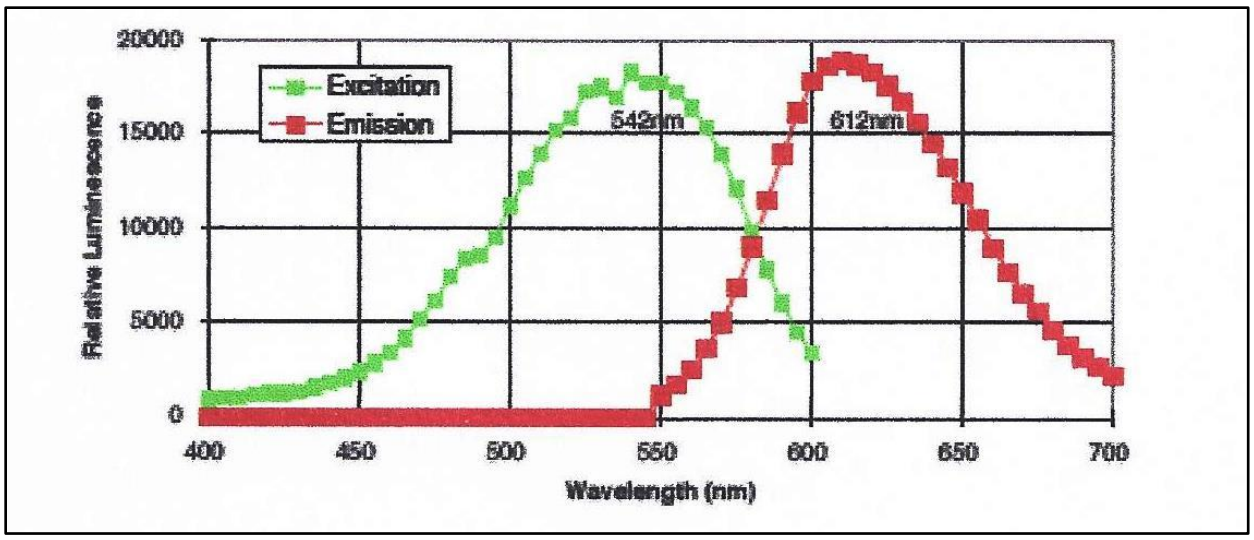

Figure 32: Red Fluorescent Polystyrene Latex Sphere Wavelength Graph (Figure Used with Permission from Thermo Fisher Scientific, 2018).

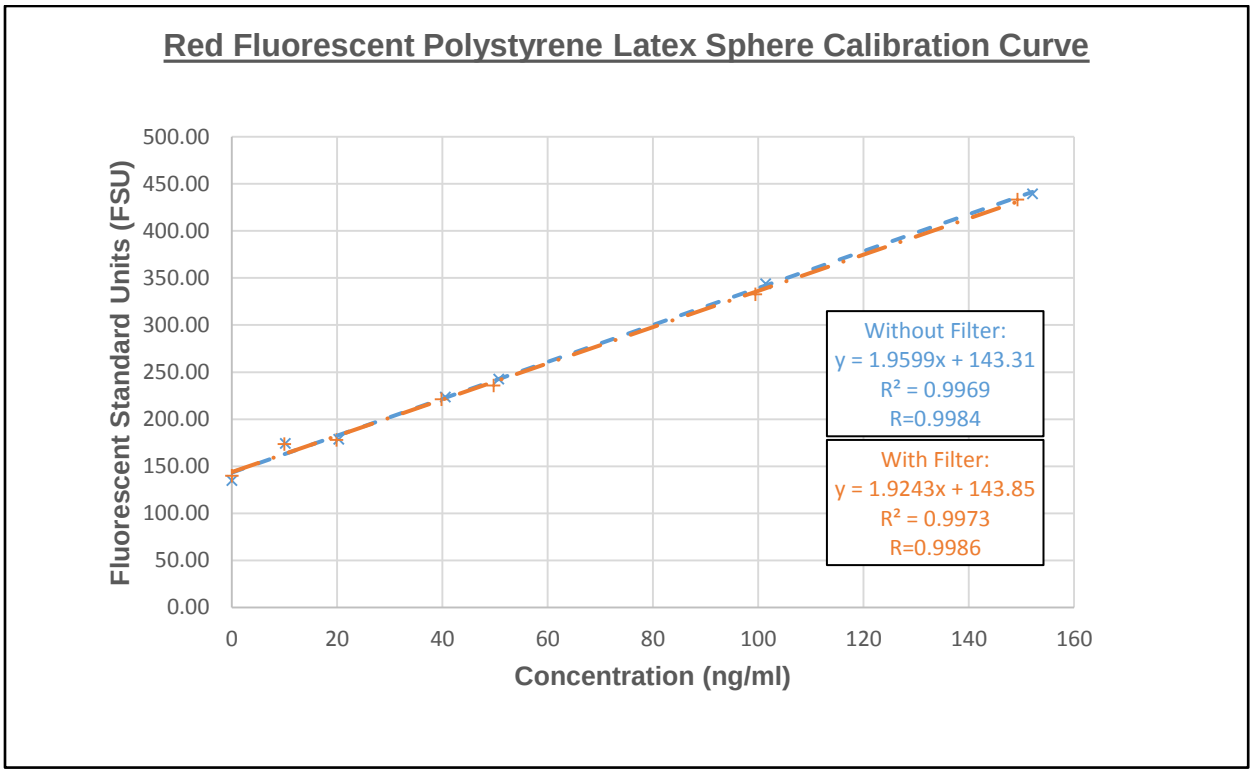

Figure 33: Red Fluorescent Polystyrene Latex Sphere Calibration Curve. (Figure Used with Permission from Liu, 2018).

Aerosol Generation from Dry Powder

Five experimental runs were conducted for both 6.0 µm and 12.0 µm particles at 0.5, 1.0, and 2.0 m/s. The first step in setting up a test run using the VAG was to activate the wind tunnel at the desired speed using the electronic controller wired to the wind tunnel fan and motor. The tunnel was allowed to run for five minutes prior to aerosol generation to ensure that air is moving through the system. During the wind tunnel warm up period, the aerosol generator was prepared for testing. To prepare the VAG, approximately 18.5 mg of the appropriate size fluorescent polystyrene dry powder was added to the VAG dust chamber. The VAG was connected to a compressed nitrogen gas line with Tygon tubing and the outlet was attached to a connection that led to the inlet of a TSI Kr-85 Radioactive Source (Shoreview, MN) which was necessary to neutralize the electrostatic charges on the airborne aerosol cloud. A connection at the outlet of the radioactive source led into the testing section of the wind tunnel where particles are introduced into the air stream. In order to generate particles with the VAG, a calibrated compressed nitrogen tank regulator was set to 20 psi in order to generate a flow of approximately 6.0 L/min. The gas flow was monitored using a TSI Model 4140 Mass Flow Meter (Shoreview, MN).

The setting for the aerosol generator controller was determined using the Relative Unit Value Equation, Equation 5, provided in the aerosol generator's operations manual (CH Technologies, 2016):

$$\mathrm{RUV} = \frac{2.5}{FSC} * DC \qquad \text{(Equation 5)}$$

where RUV is the Relative Unit Value which corresponds to the readout on the digital controller, FSC represents the Full Scale Concentration set point in the aerosol generator

digital monitor, and DC represents the Desired Concentration needed for the study. For this study, the FSC was set at 2.5 mg/m^3 and the DC was 1.0 mg/m^3 giving a RUV of 1.000. The VAG monitor ensured that the particle concentration did not drop below the desired concentration. The aerosol generation from dry powder setup can be seen in Figure 34. To characterize the aerosol concentration produced by the VAG inside the wind tunnel, the same method previously discussed on Page 45 was used.

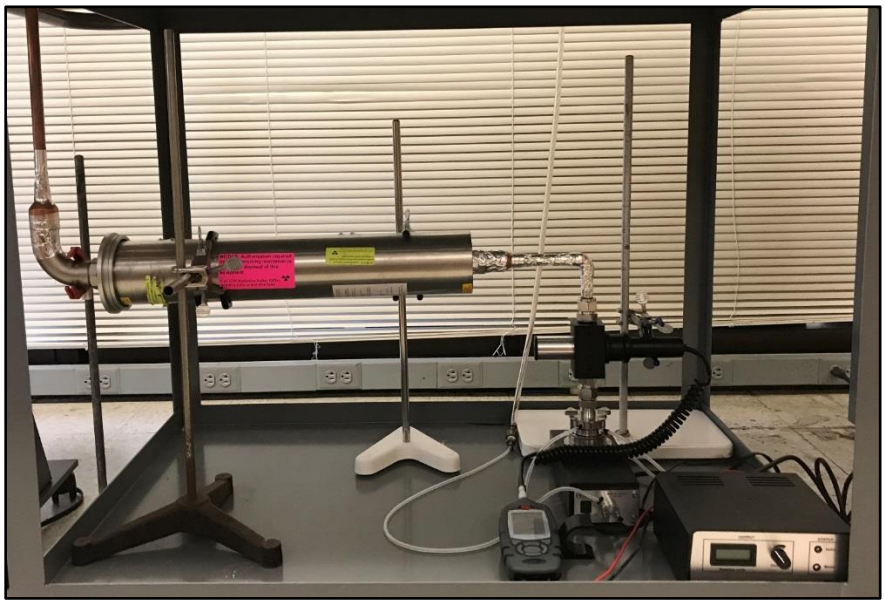

Figure 34: Aerosol Generation from Dry Powder Setup.

At the conclusion of a four hour sampling session, the wind tunnel and aerosol generator were stopped. The isokinetic sampling probe and its PVC filter were washed to determine the amount of FPLSs captured. The exposed filter was removed with tweezers and placed in a 50 ml polypropylene centrifuge tube. 10 ml of ethyl acetate was added to the centrifuge tube using a 10 ml pipet. With the tube capped, the liquid was gently shaken for 10 seconds to ensure that the walls of the centrifuge tube and filter are

coated with the solvent. The solution was allowed to sit for 20 minutes undisturbed before analysis. The inside walls of the isokinetic sampling probe were scraped with a rubber policeman to dislodge impacted particles. 10 ml of ethyl acetate were used to rinse the inside walls and the rubber policeman with the solution captured in a 50 ml polypropylene centrifuge tube. The solution was allowed to sit for 20 minutes undisturbed before analysis. Once the polystyrene latex spheres had an opportunity to dissolve and the fluorescein was in solution, the samples were analyzed using fluorometry.

The Promega GloMax Jr. Fluorometer (Madison, WI), seen in Figure 31, was used for analysis. The unit used the Promega Part E6073 Green Filter (Madison, WI) to obtain maximum detection of the red fluorescent dye that was used to coat the polystyrene latex spheres. The red fluorescent polystyrene latex sphere wavelength graph in Figure 32 shows these spheres have an excitation wavelength of 542 nm and an emission wavelength of 612. (Thermo Fisher Scientific, 2018). 190 µl of test solution was drawn up from the 50 ml centrifuge tube containing the PVC filter using a micropipette and was placed in a capillary tube for analysis. 190 µl of test solution was drawn up from the 50 ml centrifuge tube that contained the rinse from the isokinetic sampling probe wall and rubber policeman. Duplicate samples were taken from each centrifuge tube. Each individual sample was read three times and the average fluorescent standard unit value was calculated. Using the red fluorescent polystyrene latex sphere calibration curve in Figure 33, the mass of FPLSs collected was calculated.

Data Analysis

Velocity Profile

Velocity profile data was collected from all 16 quadrants of the testing section cross section. This was completed five times for each of the three selected wind velocities. Descriptive statistics such as mean, standard deviation, and coefficient of variation were calculated to help describe the data distribution. According to the United States Department of Environmental Protection, measurements should not vary more than +/- 10% in the wind tunnel testing section (United States Environmental Protection Agency, 2016a).

Turbulence Intensity

Turbulence intensity data was collected from all 16 quadrants of the testing section cross section. This was completed five times for each of the three selected wind velocities. Descriptive statistics such as mean, standard deviation, and coefficient of variation were calculated to help describe the data distribution. There are no established standards with regards to turbulence intensity in wind tunnel testing sections. It is recommended in the literature that turbulence intensity levels remain low, generally below 10% ("Boundary Conditions," 2003).

Isokinetic Sampling

Isokinetic samples were collected from five experimental runs for the four different particle sizes at the three selected wind velocities. The average mass and fluorescence were calculated. One of the main goals of the wind tunnel characterization was to

determine if particles that were introduced into the wind tunnel could be collected and detected. The fluorometric analytical method used in this study was so sensitive that the introduced fluorescent particles were detected by the instrument.

In order to determine the mass concentration of collected particles, several steps were necessary. The analytical method was developed with Xiao (Sarah) Liu, a fellow doctoral candidate in Industrial Hygiene at the University of South Florida. (Liu, 2018). The first step was to determine the average FSU for the isokinetic sampling probe filter and isokinetic sampling probe wall using the following equation:

$$FSU_{Average} = \frac{FSU_1 + FSU_2 + FSU_3}{3} \quad \text{(Equation 6)}$$

where FSU_1 is the first reading from a sampler, FSU_2 is the second reading from a sample, FSU_3 is the third reading from a sample, and $FSU_{Average}$ is the average of the three readings. The next step was to use the calibration curve and equations previously mentioned in Figure 33 to determine the analyte concentration. The equations used to determine the analyte concentration with and without the filter were as follows:

$$y = 1.9243x + 143.85 \quad \text{(Equation 7)}$$

$$y = 1.9599x + 143.31 \quad \text{(Equation 8)}$$

The calculated values were added together to get the total analyte concentration. The next step was to determine the mass of the particles collected using the following equation:

$$M_{Sample} = C_{Sample} * V_{Sample} \quad \text{(Equation 9)}$$

where M_{Sample} is the Mass Collected (ng), C_{Sample} is the concentration of Sample (ng/ml), and V_{Sample} is the Volume of Sample (ml). The final step was to determine the mass concentration of the sample using the following equation:

$$C_{Sample} = \frac{M_{Sample}}{Q_{Sample} * T_{Sample}} \quad \text{(Equation 10)}$$

where Q_{Sample} is the Sampling Flow Rate (L/min), and T_{Sample} is the Sampling Time (min). The average mass concentration, standard deviation, and coefficients of variation were calculated for each particle size at each wind speed.

Results and Discussion

The wind tunnel digital controller frequency versus the measured mean velocity along the wind tunnel centerline can be found in Table 1. Measured frequencies ranged from 1.0 Hz to 25.0 Hz. Since the wind tunnel can be run in two configurations, measurements were taken with and without the Stairmand Disk. Mean velocity with the Stairmand Disk present ranged from 0.05 m/s to 2.38 m/s and mean velocity with the Stairmand Disk absent ranged from 0.04 m/s to 2.50 m/s. This study focused on wind velocities of 0.5 m/s, 1.0 m/s, and 2.0 m/s. It should be noted that the wind tunnel was only run with the Stairmand Disk present. The corresponding frequencies with the Stairmand Disk present were 8.0 Hz, 13.0 Hz, and 22.0 Hz respectively. Figure 35 depicts graphically the relationship between mean velocity (m/s) and digital controller frequency (Hz).

Table 1: USF Wind Tunnel Fan Frequency vs. Mean Velocity

Fan Power (Hz)	Mean Velocity (m/s) with Stairmand Disk Absent	Reynolds Number with the Stairmand Disk Absent	Mean Velocity (m/s) with Stairmand Disk Present	Reynolds Number with the Stairmand Disk Present
1	0.04	694	0.05	868
2	0.07	1215	0.09	1562
3	0.13	2256	0.14	2430
4	0.18	3124	0.19	3298
5	0.25	4339	0.28	4860
6	0.33	5728	0.33	5728
7	0.42	7290	0.42	7290
8	0.50	8678	0.50	8678

Table 1 (Continued): USF Wind Tunnel Fan Frequency vs. Mean Velocity

Fan Power (Hz)	Mean Velocity (m/s) with Stairmand Disk Absent	Reynolds Number with the Stairmand Disk Absent	Mean Velocity (m/s) with Stairmand Disk Present	Reynolds Number with the Stairmand Disk Present
9	0.60	10414	0.59	10240
10	0.69	11976	0.69	11976
11	0.80	13885	0.80	13885
12	0.91	15795	0.90	15621
13	1.03	17877	1.01	17530
14	1.16	20134	1.14	19787
15	1.28	22217	1.25	21696
16	1.41	24473	1.37	23779
17	1.53	26556	1.47	25514
18	1.65	28639	1.60	27771
19	1.77	30721	1.70	29506
20	1.89	32804	1.82	31589
21	2.01	34887	1.91	33151
22	2.14	37143	2.04	35408
23	2.26	39226	2.15	37317
24	2.38	41309	2.27	39400
25	2.50	43392	2.38	41309

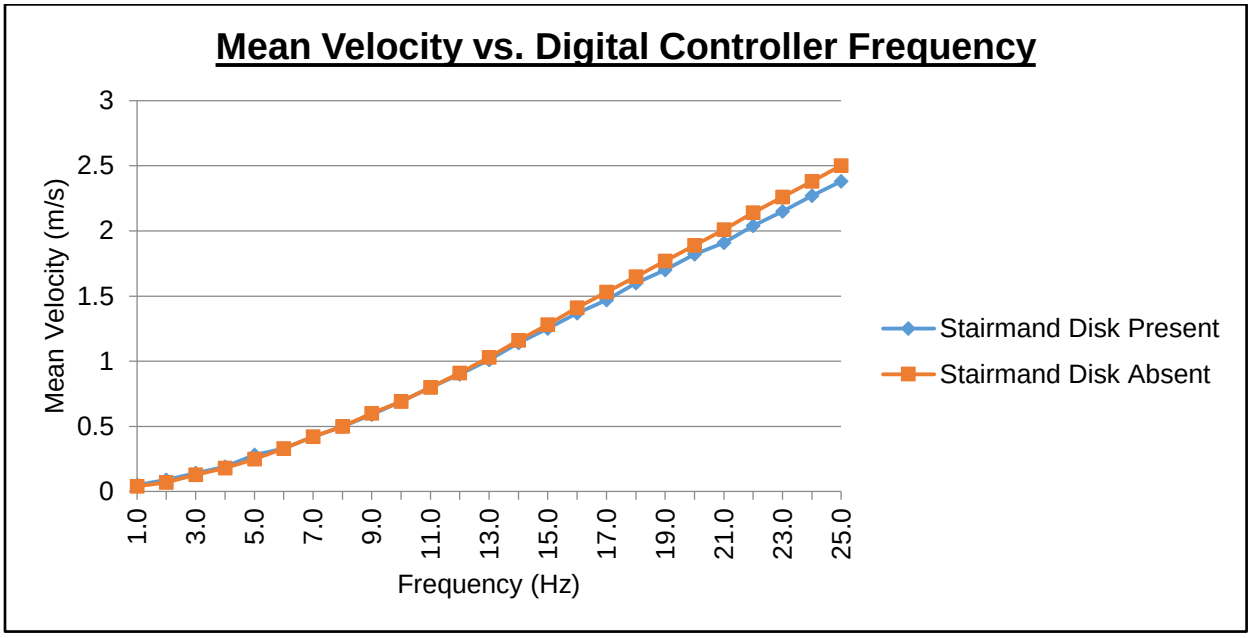

Figure 35: Velocity vs. Digital Controller Frequency Graph.

Velocity Profile

Before any measurements were taken for velocity profile and turbulence intensity, environmental conditions were recorded each day. For the five sampling days, the average temperature was 66.00°F, the average relative humidity was 57.80%, and the average barometric pressure was 29.98 inches. Table 2 shows the wind tunnel velocity profile measurements by quadrant at 0.5 m/s. Quadrant average wind velocity ranged from 0.44 m/s to 0.50 m/s. The overall average wind velocity of all the quadrants was 0.48 m/s, which was within the +/- 10% variance. The standard deviation was 0.02 and a coefficient of variation of 3.91%.

Table 2: USF Wind Tunnel Velocity Profile at 0.5 m/s

	Wind Tunnel Testing Section Ceiling				
Wind Tunnel Testing Section Left Wall	0.50	0.49	0.45	0.47	**Wind Tunnel Testing Section Right Wall**
	0.50	0.50	0.48	0.44	
	0.49	0.50	0.50	0.47	
	0.50	0.49	0.49	0.47	
	Wind Tunnel Testing Section Floor				
Overall Average = 0.48 m/s					
Standard Deviation = 0.02					
CV = 3.91%					

Quadrant 3's average velocity profile measurement was right at the lower variance limit while Quadrant 8's average velocity profile measurement was slightly below the lower variance limit. Quadrant 3 is located towards the ceiling of the wind tunnel while Quadrant 8 is located on the outside wall of the wind tunnel. The isokinetic sampling probe used in this study was centered horizontally and vertically along the wind tunnel centerline where all quadrant average velocity profile measurements were within

acceptable limits. In addition, the overall average wind velocity of all the quadrants was within the +/- 10% variance.

As previously indicated, the isokinetic sampling probe was centered horizontally and vertically along the wind tunnel testing section centerline. Velocity profile data was normalized for each wind velocity tested to determine if there were any large scale differences in specific quadrants from the wind tunnel testing section centerline measurement. Table 3 shows the normalized wind tunnel velocity profile measurements by quadrant at 0.5 m/s. The normalized data showed that wind velocities in quadrants along the outside wall of the wind tunnel testing section varied more from the centerline velocity measurement than those quadrants found in the center of the wind tunnel testing section. This variability is expected because of the shape of the velocity profile in the wind tunnel testing section.

Table 3: Normalized USF Wind Tunnel Velocity Profile at 0.5 m/s

	Wind Tunnel Testing Section Ceiling				
Wind Tunnel Testing Section Left Wall	0.99	0.98	0.90	0.94	**Wind Tunnel Testing Section Right Wall**
	1.00	1.00	0.95	0.88	
	0.97	1.00	1.00	0.94	
	0.99	0.98	0.98	0.93	
	Wind Tunnel Testing Section Floor				
Velocity at Wind Tunnel Centerline = 0.50 m/s					

Table 4 shows the wind tunnel velocity profile measurements by quadrant at a target wind velocity of 1.0 m/s. Quadrant average wind velocities ranged from 0.97 m/s to 1.03 m/s. The overall average wind velocity of all the quadrants was 1.00 m/s, which

within the +/- 10% variance. The standard deviation was 0.02 and a coefficient of variation of 1.72%.

Table 4: USF Wind Tunnel Velocity Profile at 1.0 m/s.

	Wind Tunnel Testing Section Ceiling				
Wind Tunnel Testing Section Left Wall	1.03	0.97	0.98	0.99	Wind Tunnel Testing Section Right Wall
	1.01	1.00	1.00	1.00	
	1.00	1.01	1.01	0.99	
	1.01	1.03	1.03	1.00	
	Wind Tunnel Testing Section Floor				
Overall Average = 1.00 m/s					
Standard Deviation = 0.02					
CV = 1.72%					

The overall average wind velocity with the digital controller set at 1.0 m/s was 1.00 m/s, which was within the +/- 10% variance. The isokinetic sampling probe used in this study was centered horizontally and vertically along the wind tunnel centerline where all average velocity profile measurements were within acceptable limits.

Similarly, Table 5 shows the normalized wind tunnel velocity profile measurements by quadrant at 1.0 m/s. The normalized data showed that wind velocities in quadrants along the outside wall of the wind tunnel testing section varied more than quadrants found in the center of the wind tunnel testing section.

Table 5: Normalized USF Wind Tunnel Velocity Profile at 1.0 m/s

	Wind Tunnel Testing Section Ceiling				
Wind Tunnel Testing Section Left Wall	1.02	0.96	0.97	0.98	Wind Tunnel Testing Section Right Wall
	1.00	0.99	0.99	0.99	
	0.99	1.00	1.00	0.98	
	1.00	1.02	1.02	0.99	
	Wind Tunnel Testing Section Floor				
Velocity at Wind Tunnel Centerline = 1.01 m/s					

Table 6 shows the wind tunnel velocity profile measurements by quadrant at a target wind velocity of 2.0 m/s. The quadrant average wind velocity ranged from 1.97 m/s to 2.07 m/s. The overall average wind velocity of all the quadrants was 2.04 m/s with a standard deviation of 0.05, and a coefficient of variation of 2.44%.

Table 6: USF Wind Tunnel Velocity Profile at 2.0 m/s

	Wind Tunnel Testing Section Ceiling				
Wind Tunnel Testing Section Left Wall	2.01	1.98	2.07	2.02	Wind Tunnel Testing Section Right Wall
	2.03	1.97	2.07	2.07	
	2.02	1.97	2.07	2.09	
	1.99	2.07	2.11	2.12	
	Wind Tunnel Testing Section Floor				
Overall Average = 2.04 m/s					
Standard Deviation = 0.05					
CV = 2.44%					

The overall average wind velocity with the digital controller set at 2.0 m/s was 2.04 m/s, which was within the +/- 10% variance. The isokinetic sampling probe used in this

study was centered horizontally and vertically along the wind tunnel centerline where all average velocity profile measurements were within acceptable limits.

Table 7 shows the normalized wind tunnel velocity profile measurements by quadrant at 2.0 m/s. Similarly, the normalized data showed that wind velocities in quadrants along the outside wall of the wind tunnel testing section varied more than quadrants found in the center of the wind tunnel testing section.

Table 7: Normalized USF Wind Tunnel Velocity Profile at 1.0 m/s

	Wind Tunnel Testing Section Ceiling				
Wind Tunnel Testing Section Left Wall	0.99	0.97	1.02	0.99	**Wind Tunnel Testing Section Right Wall**
	0.99	0.96	1.01	1.01	
	0.99	0.97	1.02	1.02	
	0.97	1.02	1.04	1.04	
	Wind Tunnel Testing Section Floor				
Velocity at Wind Tunnel Centerline = 2.04 m/s					

Air flowing through a duct, regardless of whether it is circular or rectangular, is known to have different velocities depending on location in the duct. Burgess et. al (2004) explains that air moving through a duct has lower velocities measured against the walls when compared to air flowing at maximum velocity in the center of the duct. Air flowing close to the walls experiences shear stresses resulting in frictional losses. (Burgess et. al, 2004). This phenomenon may explain why the average velocity profile measurement at 0.5 m/s for Quadrant 3 (Upper Wall) was right at the lower variance limit and why the average velocity profile measurement for Quadrant 8 (Right Wall) was slightly below the lower variance limit at 0.5 m/s. While all measurements were within the allowable variance at 1.0 m/s and 2.0 m/s, this phenomenon may explain variations in the data at

those wind velocities. This variability is expected because of the shape of the velocity profile in the wind tunnel testing section.

Turbulence Intensity

Since turbulence intensity measurements were taken simultaneously with velocity profile measurements, data related to the environmental conditions were the same as those mentioned previously. Much like the velocity profile measurements, turbulence intensity measurements fluctuated depending on quadrant location inside the wind tunnel testing section. Regardless of wind velocity, turbulence intensity measurements followed the same pattern. Measurements taken along the outside walls of the wind tunnel testing section tended to be higher sometimes above the 10% threshold while those measurements taken in the central quadrants of the wind tunnel testing section tended to be lower, often below the 10% threshold. Like with the velocity profile measurements, the interior quadrants of the wind tunnel testing section were of particular importance because the isokinetic sampling probe used for particle collection was centered vertically and horizontally in this area.

Table 8 shows the wind tunnel turbulence intensity profile measurements by quadrant at 0.5 m/s. The target turbulence intensity was below 10% with the 16 individual quadrant average turbulence intensities ranging from 6% to 12%. The overall average turbulence intensity was 9% with a standard deviation of 1.71, and a coefficient of variation of 19.06%. Quadrant average turbulence intensity measurements along the walls of the wind tunnel testing section tended to be higher while central measurements of the wind tunnel testing section were below the 10% threshold. This is expected as stated before, due to natural profile of the velocity in the wind tunnel testing section.

Table 8: USF Wind Tunnel Turbulence Intensity Profile at 0.5 m/s

	Wind Tunnel Testing Section Ceiling				
Wind Tunnel Testing Section Left Wall	10	9	8	10	Wind Tunnel Testing Section Right Wall
	10	7	8	12	
	9	6	7	9	
	11	8	8	12	
	Wind Tunnel Testing Section Floor				
Overall Average = 9%					
Standard Deviation = 1.71					
CV = 19.06%					

Like the velocity profile measurements, the turbulence intensity measurements were normalized for each wind velocity tested to determine if there were any large scale differences in specific quadrants from the wind tunnel testing section centerline measurement. Table 9 shows the normalized wind tunnel turbulence intensity profile at 0.5 m/s. The normalized data showed that turbulence intensity in quadrants along the outside wall of the wind tunnel testing section varied more from the centerline turbulence intensity measurement than those quadrants found in the interior of the wind tunnel testing section.

Table 9: Normalized USF Wind Tunnel Turbulence Intensity Profile at 0.5 m/s

	Wind Tunnel Testing Section Ceiling				
Wind Tunnel Testing Section Left Wall	1.5	1.2	1.2	1.5	Wind Tunnel Testing Section Right Wall
	1.4	1.0	1.1	1.7	
	1.2	0.9	1.0	1.3	
	1.6	1.1	1.1	1.7	
	Wind Tunnel Testing Section Floor				
Turbulence Intensity at Wind Tunnel Centerline = 7%					

Table 10 shows the wind tunnel turbulence intensity profile measurements by quadrant at 1.0 m/s. The target turbulence intensity was below 10% with the 16 individual quadrant average turbulence intensities ranging from 7% to 13%. The overall average among all the quadrants was 10% with a standard deviation of 1.72, and a coefficient of variation of 17.29%. Quadrant average turbulence intensity measurements along the walls of the wind tunnel testing section tended to be higher while measurements in the center of the wind tunnel testing section were below the 10% threshold.

Table 10: USF Wind Tunnel Turbulence Intensity Profile at 1.0 m/s.

	Wind Tunnel Testing Section Ceiling				
Wind Tunnel Testing Section Left Wall	12	10	9	11	**Wind Tunnel Testing Section Right Wall**
	12	8	8	12	
	10	7	8	11	
	12	9	9	13	
	Wind Tunnel Testing Section Floor				
Overall Average = 10%					
Standard Deviation = 1.72					
CV = 17.29%					

Table 11 shows the normalized wind tunnel turbulence intensity profile at 1.0 m/s. The normalized data showed that turbulence intensity in quadrants adjacent to the outside wall of the wind tunnel testing section varied more than the centerline turbulence intensity of the wind tunnel testing section.

Table 11: Normalized USF Wind Tunnel Turbulence Intensity Profile at 1.0 m/s

	Wind Tunnel Testing Section Ceiling				
Wind Tunnel Testing Section Left Wall	1.7	1.4	1.3	1.6	Wind Tunnel Testing Section Right Wall
	1.7	1.1	1.2	1.7	
	1.4	1.0	1.2	1.5	
	1.7	1.3	1.3	1.9	
	Wind Tunnel Testing Section Floor				
Turbulence Intensity at Wind Tunnel Centerline = 7%					

Table 12 shows the wind tunnel turbulence intensity profile measurements by quadrant at 2.0 m/s. The target turbulence intensity was below 10% with the 16 individual quadrant average turbulence intensities ranging from 5% to 11%. The overall average among all the quadrants was 8% with a standard deviation of 1.69, and a coefficient of variation of 21.46%. Quadrant average turbulence intensity measurements along the walls of the wind tunnel testing section tended to be higher while measurements in the central quadrants of the wind tunnel testing section were below the 10% threshold.

Table 12: USF Wind Tunnel Turbulence Intensity Profile at 2.0 m/s

	Wind Tunnel Testing Section Ceiling				
Wind Tunnel Testing Section Left Wall	10	7	7	10	Wind Tunnel Testing Section Right Wall
	9	6	6	9	
	8	5	6	8	
	10	7	7	11	
	Wind Tunnel Testing Section Floor				
Overall Average = 8%					
Standard Deviation = 1.69					
CV = 21.46%					

Table 13 shows the normalized wind tunnel turbulence intensity profile at 2.0 m/s. The normalized data showed that turbulence intensity in quadrants adjacent to the outside wall of the wind tunnel testing section varied more than the centerline turbulence intensity of the wind tunnel testing section.

.

Table 13: Normalized USF Wind Tunnel Turbulence Intensity Profile at 2.0 m/s

	Wind Tunnel Testing Section Ceiling				
Wind Tunnel Testing Section Left Wall	1.7	1.1	1.2	1.7	**Wind Tunnel Testing Section Right Wall**
	1.4	1.1	1.0	1.6	
	1.3	0.9	0.9	1.3	
	1.6	1.2	1.2	1.8	
	Wind Tunnel Testing Section Floor				
Turbulence Intensity at Wind Tunnel Centerline = 6%					

All attempts were made to design the wind tunnel so that it had the lowest turbulence intensity possible. While some average turbulence intensity measurements were above the 10% threshold, these measurements were not in the location of the isokinetic sampling probe. It should also be noted that while some individual quadrant average turbulence intensity measurements were above the 10% threshold at the different wind velocities, the overall turbulence intensity for the wind tunnel testing section at each wind velocity was at or below 10%. During the design phase of the wind tunnel, all components were designed so that the assembled wind tunnel would fit in the assigned laboratory on the university campus. It is possible that lengthening the wind tunnel testing section could allow additional distance for air patterns inside the wind tunnel testing section to reach a more uniform pattern thereby decreasing turbulence intensity.

Increasing the overall size of the wind tunnel was not possible due to the allocated current location.

Isokinetic Sampling

Before any isokinetic sampling measurements were taken, environmental conditions were recorded each day. For the 60 sampling days, the average temperature was 58.93°F, the average relative humidity was 66.25%, and the average barometric pressure was 30.14 inches. Table 14 shows isokinetic sampling data for 0.5 µm particles at 0.5 m/s. The fluorescence ranged from 452.34 FSU to 551.04 FSU while the mass concentration ranged from 0.000632 ng/ml to 0.000767 ng/ml. The average fluorescence was 497.89 FSU and the average mass concentration was 0.000693 ng/ml.

Table 14: Isokinetic Sampling Data for 0.5 µm Particles at 0.5 m/s

Isokinetic Sampling Data for 0.5 µm Particles at 0.5 m/s				
Run	**Particle Size (um)**	**Wind Velocity (m/s)**	**Fluorescence (FSU)**	**Mass Concentration (ng/ml)**
1	0.50	0.50	551.04	0.000767
2	0.50	0.50	452.34	0.000632
3	0.50	0.50	520.37	0.000725
4	0.50	0.50	499.10	0.000693
5	0.50	0.50	466.60	0.000649
Average			497.89	0.000693

Table 15 shows the isokinetic sampling data for 0.5 µm particles at 1.0 m/s. The fluorescence ranged from 398.29 FSU to 555.49 FSU while the mass concentration ranged from 0.000278 ng/ml to 0.000386 ng/ml. The average fluorescence was 448.99 FSU and the average mass concentration was 0.000312 ng/ml.

Table 15: Isokinetic Sampling Data for 0.5 µm Particles at 1.0 m/s

Isokinetic Sampling Data for 0.5 µm Particles at 1.0 m/s				
Run	**Particle Size (um)**	**Wind Velocity (m/s)**	**Fluorescence (FSU)**	**Mass Concentration (ng/ml)**
1	0.50	1.00	555.49	0.000386
2	0.50	1.00	457.84	0.000319
3	0.50	1.00	407.35	0.000284
4	0.50	1.00	398.29	0.000278
5	0.50	1.00	425.99	0.000296
Average			448.99	0.000312

Table 16 shows the isokinetic sampling data for 0.5 µm particles at 2.0 m/s. The fluorescence ranged from 264.30 FSU to 309.06 FSU while the mass concentration ranged from 0.000092 ng/ml to 0.000107 ng/ml. The average fluorescence was 289.60 and the average mass concentration was 0.000101 ng/ml.

Table 16: Isokinetic Sampling Data for 0.5 µm Particles at 2.0 m/s

Isokinetic Sampling Data for 0.5 µm Particles at 2.0 m/s				
Run	**Particle Size (um)**	**Wind Velocity (m/s)**	**Fluorescence (FSU)**	**Mass Concentration (ng/ml)**
1	0.50	2.00	309.06	0.000107
2	0.50	2.00	299.01	0.000104
3	0.50	2.00	304.84	0.000106
4	0.50	2.00	270.78	0.000094
5	0.50	2.00	264.30	0.000092
Average			289.60	0.000101

Table 17 shows the isokinetic sampling data for 2.0 µm at 0.5 m/s. The fluorescence ranged from 281.14 FSU to 532.67 FSU while the mass concentration ranged from 0.000390 ng/ml to 0.000735 ng/ml. The average fluorescence was 425.34 FSU and the average mass concentration was 0.000589 ng/ml.

Table 17: Isokinetic Sampling Data for 2.0 µm Particles at 0.5 m/s

Isokinetic Sampling Data for 2.0 µm Particles at 0.5 m/s				
Run	**Particle Size (um)**	**Wind Velocity (m/s)**	**Fluorescence (FSU)**	**Mass Concentration (ng/ml)**
1	2.00	0.50	493.44	0.000683
2	2.00	0.50	532.67	0.000735
3	2.00	0.50	482.95	0.000669
4	2.00	0.50	336.51	0.000467
5	2.00	0.50	281.14	0.000390
Average			425.34	0.000589

Table 18 shows the isokinetic sampling data for 2.0 µm particles at 1.0 m/s. The fluorescence ranged from 228.81 FSU to 958.07 FSU while the mass concentration ranged from 0.000158 ng/ml to 0.000667 ng/ml. The average fluorescence was 471.25 FSU and the average mass concentration was 0.000327 ng/ml.

Table 18: Isokinetic Sampling Data for 2.0 µm Particles at 1.0 m/s

Isokinetic Sampling Data for 2.0 µm Particles at 1.0 m/s				
Run	**Particle Size (um)**	**Wind Velocity (m/s)**	**Fluorescence (FSU)**	**Mass Concentration (ng/ml)**
1	2.00	1.00	410.73	0.000284
2	2.00	1.00	958.07	0.000667
3	2.00	1.00	358.95	0.000248
4	2.00	1.00	399.69	0.000276
5	2.00	1.00	228.81	0.000158
Average			471.25	0.000327

Table 19 shows the isokinetic sampling data for 2.0 µm particles at 2.0 m/s. The fluorescence ranged from 246.90 FSU to 347.88 FSU while the mass concentration ranged from 0.000085 ng/ml to 0.000120 ng/ml. The average fluorescence was 285.12 FSU and the average mass concentration was 0.000099 ng/ml.

Table 19: Isokinetic Sampling Data for 2.0 µm Particles at 2.0 m/s

Isokinetic Sampling Data for 2.0 µm Particles at 2.0 m/s				
Run	**Particle Size (um)**	**Wind Velocity (m/s)**	**Fluorescence (FSU)**	**Mass Concentration (ng/ml)**
1	2.00	2.00	347.88	0.000120
2	2.00	2.00	297.26	0.000103
3	2.00	2.00	246.90	0.000085
4	2.00	2.00	260.67	0.000090
5	2.00	2.00	272.88	0.000094
Average			285.12	0.000099

Table 20 shows the isokinetic sampling data for 6.0 µm particles at 0.5 m/s. The fluorescence ranged from 1149.07 FSU to 4008.52 FSU while the mass concentration ranged from 0.001609 ng/ml to 0.005624 ng/ml. The average fluorescence was 1927.84 FSU and the average mass concentration was 0.002703 ng/ml.

Table 20: Isokinetic Sampling Data for 6.0 µm Particles at 0.5 m/s

Isokinetic Sampling Data for 6.0 µm Particles at 0.5 m/s				
Run	**Particle Size (um)**	**Wind Velocity (m/s)**	**Fluorescence (FSU)**	**Mass Concentration (ng/ml)**
1	6.00	0.50	4008.52	0.005624
2	6.00	0.50	2030.45	0.002844
3	6.00	0.50	1149.07	0.001609
4	6.00	0.50	1188.15	0.001668
5	6.00	0.50	1263.01	0.001770
Average			1927.84	0.002703

Table 21 shows the isokinetic sampling data for 6.0 µm particles at 1.0 m/s. The fluorescence ranged from 1249.06 FSU to 1500.17 FSU while the mass concentration ranged from 0.000874 ng/ml to 0.001048 ng/ml. The average fluorescence was 1374.27 FSU and the average mass concentration was 0.000961 ng/ml.

Table 21: Isokinetic Sampling Data for 6.0 µm Particles at 1.0 m/s

Isokinetic Sampling Data for 6.0 µm Particles at 1.0 m/s				
Run	**Particle Size (um)**	**Wind Velocity (m/s)**	**Fluorescence (FSU)**	**Mass Concentration (ng/ml)**
1	6.00	1.00	1407.78	0.000984
2	6.00	1.00	1378.40	0.000964
3	6.00	1.00	1335.95	0.000933
4	6.00	1.00	1500.17	0.001048
5	6.00	1.00	1249.06	0.000874
Average			1374.27	0.000961

Table 22 shows the isokinetic sampling data for 6.0 µm particles at 2.0 m/s. The fluorescence ranged from 801.46 FSU to 1000.21 FSU while the mass concentration ranged from 0.000280 ng/ml to 0.000350 ng/ml. The average fluorescence was 866.85 FSU and the average mass concentration was 0.000303 ng/ml.

Table 22: Isokinetic Sampling Data for 6.0 µm Particles at 2.0 m/s

Isokinetic Sampling Data for 6.0 µm Particles at 2.0 m/s				
Run	**Particle Size (um)**	**Wind Velocity (m/s)**	**Fluorescence (FSU)**	**Mass Concentration (ng/ml)**
1	6.00	2.00	842.61	0.000295
2	6.00	2.00	826.75	0.000289
3	6.00	2.00	801.46	0.000280
4	6.00	2.00	1000.21	0.000350
5	6.00	2.00	863.24	0.000302
Average			866.85	0.000303

Table 23 shows the isokinetic sampling data for 12.0 µm particles at 0.5 m/s. The fluorescence ranged from 213.37 FSU to 294.40 FSU while the mass concentration ranged from 0.000296 ng/ml to 0.000412 ng/ml. The average fluorescence was 257.29 FSU and the average mass concentration was 0.000358 ng/ml.

Table 23: Isokinetic Sampling Data for 12.0 µm Particles at 0.5 m/s

Isokinetic Sampling Data for 12.0 µm Particles at 0.5 m/s				
Run	**Particle Size (um)**	**Wind Velocity (m/s)**	**Fluorescence (FSU)**	**Mass Concentration (ng/ml)**
1	12.00	0.50	294.40	0.000412
2	12.00	0.50	291.21	0.000406
3	12.00	0.50	250.12	0.000349
4	12.00	0.50	237.37	0.000330
5	12.00	0.50	213.37	0.000296
Average			257.29	0.000358

Table 24 shows the isokinetic sampling data for 12.0 µm particles at 1.0 m/s. The fluorescence ranged from 278.55 FSU to 368.92 FSU while the mass concentration ranged from 0.000194 ng/ml to 0.000256 ng/ml. The average fluorescence was 327.86 FSU and the average mass concentration was 0.000228 ng/ml.

Table 24: Isokinetic Sampling Data for 12.0 µm Particles at 1.0 m/s

Isokinetic Sampling Data for 12.0 µm Particles at 1.0 m/s				
Run	**Particle Size (um)**	**Wind Velocity (m/s)**	**Fluorescence (FSU)**	**Mass Concentration (ng/ml)**
1	12.00	1.00	356.90	0.000249
2	12.00	1.00	368.92	0.000256
3	12.00	1.00	335.26	0.000233
4	12.00	1.00	299.69	0.000209
5	12.00	1.00	278.55	0.000194
Average			327.86	0.000228

Table 25 shows the isokinetic sampling data for 12.0 µm particles at 2.0 m/s. The fluorescence ranged from 107.04 FSU to 236.91 FSU and the mass concentration ranged from 0.000037 ng/ml to 0.000082 ng/ml. The average fluorescence was 145.66 FSU and the average mass concentration was 0.000050 ng/ml.

Table 25: Isokinetic Sampling Data for 12.0 µm Particles at 2.0 m/s

Isokinetic Sampling Data for 12.0 µm Particles at 2.0 m/s				
Run	**Particle Size (um)**	**Wind Velocity (m/s)**	**Fluorescence (FSU)**	**Mass Concentration (ng/ml)**
1	12.00	2.00	107.04	0.000037
2	12.00	2.00	121.40	0.000042
3	12.00	2.00	109.78	0.000038
4	12.00	2.00	153.16	0.000053
5	12.00	2.00	236.91	0.000082
Average			145.66	0.000050

As previously discussed the BLAM was used to generate aerosols from liquid suspensions composed of 0.5 µm and 2.0 µm particles. Fluorescence was detected in all 0.5 µm and 2.0 µm samples. At 0.5 m/s, the 0.5 µm particles were detected at a higher fluorescence and mass concentration at Run 1, declining slightly at Run 2, rising slightly at Run 3, before plateauing through Run 5 (Table 14) while fluorescence levels and mass concentration for the 2.0 µm particles were relatively consistent through Run 3 before gradually declining through Run 5 (Table 15). At 1.0 m/s, the 0.5 µm particles peaked in fluorescence and mass concentration at Run 1 declining through Run 4 before rising slightly at Run 5 (Table 16) while fluorescence levels and mass concentration for the 2.0 µm particles peaked at Run 2, before declining through Run 5 (Table 17). At 2.0 m/s, the 0.5 µm particles fluorescence and mass concentration remained relatively consistent from Run 1 to Run 3 before declining slightly through Run 5 (Table 18) while fluorescence levels and mass concentration for the 2.0 µm particles peaked at Run 1, declined through Run 3, before plateauing through Run 5 (Table 19). For the three wind velocities tested, 0.5 µm particles had a higher fluorescence and mass concentration when compared to 2.0 µm particles. While the same analytical procedure and calibration curve were used, there was some variability in detected fluorescence levels and calculated mass

concentration. To help reduce variability, the BLAM was cleaned with a mild detergent and allowed to air dry after each use. Before switching to a new particle size the BLAM was placed in an ultrasonic bath to thoroughly clean the instrument.

As previously discussed the VAG was used to generate aerosols from liquid suspensions composed of 6.0 µm and 12.0 µm particles. Fluorescence was detected in all 6.0 µm and 12.0 µm samples. At 0.5 m/s, the 6.0 µm particles were detected at a higher fluorescence and mass concentration at Run 1 with rapidly declining levels through Run 3 before rising slightly through Run 5 (Table 20) while fluorescence levels and mass concentration for the 12.0 µm particles gradually declined from Run 1 to Run 5 (Table 21). At 1.0 m/s, the 6.0 µm particles experienced a slight decrease in fluorescence and mass concentration from Run 1 to Run 3 before peaking at Run 4 then declining again at Run 5 (Table 22) while fluorescence levels and mass concentration for the 12.0 µm particles rose slightly from Run 1 to Run 2 before declining through Run 5 (Table 23). At 2.0 m/s, the 6.0 µm particles experienced a slight decrease in fluorescence and mass concentration from Run 1 to Run 3 before peaking at Run 4 then declining again at Run 5 (Table 24) while fluorescence levels and mass concentration for the 12.0 µm particles rose slightly from Run 1 to Run 2, declined slightly at Run 3, before rising through Run 5 (Table 25). For the three wind velocities tested, 6.0 µm particles had a higher fluorescence and mass concentration when compared to 12.0 µm particles. While the same analytical procedure and calibration curve were used, there was some variability in detected fluorescence levels and mass concentration. When the VAG runs period of time, dry powder in the VAG dust chamber gets depleted and more must be added so that the instrument can maintain desired concentration levels. During this study, dry powder was

added to the VAG dust chamber before every experimental run. When breaking down the VAG for cleaning, the deagglomeration assembly was found to be loaded with a large amount of dry powder. It is possible that this accumulation of powder may have affected the operating efficiency of the VAG and therefore the variability. Before switching to a new particle size the VAG was cleaned with a mild detergent and each component was placed in an ultrasonic bath to thoroughly clean the instrument.

Study Strengths

Throughout the study planning process, all attempts were made to identify best practices that would ensure success while also identifying potential pitfalls. Several strengths and limitations became apparent at the conclusion of this research study. One of the major strengths of this study were that all aspects of the wind tunnel design were driven by information obtained during the literature review of scientific information. This guaranteed that the different vendors responsible for building the different components were given blueprints with proper specifications to produce optimum results. Extreme care was taken during the assembly of the wind tunnel so that none of the delicate parts were damaged. Because great care and attention were taken during the design phase of the wind tunnel, the velocity profile, turbulence intensity, and isokinetic sampling data generated during this study proved that it performs as desired.

Another strength of this study was the use of a very sensitive analytical method. Fluorometry has been widely used in science due to its sensitivity and reliability. (Chen et. al, 2004; Lindsley et. al, 2006; Su et. al, 2012) All of the nitrogen gas used to generate and transport our test aerosol was HEPA filtered. The use of HEPA filters at the entrance and exit of the tunnel insured that there was no interference from airborne particles in

laboratory air. In addition, the fluorometer would only detect the fluorescent material and not the ambient particles. The analytical procedures were so sensitive that it was possible to detect mass concentrations as low as ng/ml.

A final strength of this study was the innovative use of the two new aerosol generators that were not previously used in this type of application. Based on the literature review, the BLAM had only been used in an aerosol generator comparison study interested in biological agents and in a rodent inhalation study examining biological agent exposure while the VAG had only been used to assess the toxicity of lunar dust and in pharmaceutical trials focused on aerosolizing certain medications. (Rissler et al., 2009; Lam et al., 2013; Scully et al., 2013; Zhen et al., 2014; Bowling, 2016, and Li et al., 2017) The successful use of these two aerosol generators in this application constitutes a major contribution to the scientific community.

Study Limitations

While this study had several strengths, it was not without its limitations. One limitation was that in this study airborne aerosols were only sampled with a blunt isokinetic sampling probe facing directly into the air stream. A tapered, thin walled sampling probe should be utilized in future studies. Future studies may also aim to examine aerosol collection efficiencies with the isokinetic sampling probe or another industrial hygiene sampler at different orientations such as 45°, 90°, and 180°. This may provide insight into collection efficiencies when the airstream is approaching a sampling instrument from a different direction. There have been many studies reported in the literature where sampler orientation and collection efficiencies were examined. Su et. al (2012) varied the orientation of the NIOSH Two-Stage Bioaerosol Sampler in a wind tunnel and did not find

any significant effect on aspiration efficiencies. Further study may be needed to see if similar results are obtained.

One of the aims of this study was to introduce, collect, and detect FPLSs in the wind tunnel testing section. Comparison of the aerosol concentration introduced into the wind tunnel testing section to the amount collected was not completed in this study. To accomplish this, the wind tunnel testing section would need to be modified to incorporate a particle counter or cascade impactor. A particle counter or cascade impactor would allow a researcher to quantify the actual particle size distribution and concentration introduced inside the wind tunnel over the course of a sampling period. By sampling isokinetically using a method similar to the one in this study, a researcher could collect and determine the concentration of particles collected and compare it to what is captured by the particle counter or cascade impactor. This may give insight into sampling method and aerosol generator efficiency.

Conclusions

The aims of this study were to design a new wind tunnel using best practices reported in the scientific literature, construct it using high quality material from reliable vendors, and characterize its performance characteristics by measuring the velocity profile, the turbulence intensity profile, and by sampling of aerosols isokinetically. The data generated from this study demonstrates that the aims and objectives were successfully met.

Future Research

Now that a wind tunnel exists on the University of South Florida campus, new research into aerosol behavior under moving air conditions is possible. This project has stimulated several possible ideas for future endeavors. One idea for future research would be to use computational fluid dynamics and engineering computer software to examine a theoretical model using the exact parameters of our wind tunnel. Once theoretical model data is available, it could be compared to the actual data that was collected in this study. Several studies have utilized computational fluid dynamics to validate wind tunnel construction. (Abdelhamed et al., 2015 and Siddique, 2012)

Simultaneous isokinetic sampling at different points of the wind tunnel testing section cross section would provide useful information. This study focused on isokinetic sampling along the wind tunnel centerline with the probe centered horizontally and vertically. It would be valuable to conduct isokinetic sampling at various points in the same vertical plane to quantify spatial variations of the aerosol distribution within the wind

tunnel testing section. Because wind patterns tend to vary in different areas of a wind tunnel testing section, the possibility exists that aerosol concentrations could vary as well. A study conducted in 2013 using isokinetic sampling at five different points in the same vertical plane of a wind tunnel testing section and found that there were some fluctuations in aerosol distribution, sometimes over 10%. (Lee et al., 2013) It should be noted that this study only used an isokinetic sampling probe for aerosol collection. Future studies may aim to evaluate active or passive samplers in the wind tunnel testing section.

The utility of this new wind tunnel cannot be understated. While development of this wind tunnel has purposes rooted in industrial hygiene research, it can also be used in studies related to air pollution and environmental health. Results collected during this research indicate that the University of South Florida wind tunnel was designed and constructed appropriately. It can now successfully be used by researchers interested in evaluating industrial hygiene equipment and instrumentation with monodisperse aerosols ranging from 0.5 µm to 12.0 µm in moving air with velocities ranging from 0.5 m/s to 2.0 m/s.

References

Abdelhamed, A. S., Yassen, Y. E.-S., & ElSakka, M. M. (2015). Design optimization of three dimensional geometry of wind tunnel contraction. *Ain Shams Engineering Journal, 6*(1), 281-288. doi:http://dx.doi.org/10.1016/j.asej.2014.09.008

Air Techniques International. (2016). Upstream Challenge Aerosol Introduction Point. Retrieved from http://www.atitest.com/knowledge-center/faqs/faq003-upstream-challenge-aerosol-introduction-point/

Ayres, J. (2002). Chronic effects of air pollution: BMJ Publishing Group Ltd.

Baccini, M., Mattei, A., Mealli, F., Bertazzi, P. A., & Carugno, M. (2017). Assessing the short term impact of air pollution on mortality: a matching approach. *Environmental Health, 16*(1), 7.

Baldwin, P. E., & Maynard, A. D. (1998). A survey of wind speeds in indoor workplaces. *Ann Occup Hyg, 42*(5), 303-313.

Barlow, J. B., Rae II, W. H., & Pope, A. (1999). *Low-Speed Wind Tunnel Testing* (Third ed.): John Wiley & Sons.

Baron, P., & John, W. (1999). Sampling for Thoracic Aerosol. In J. H. Vincent (Ed.), *Particle Size-Selective Sampling of Particulate Air Contaminants* (pp. 141-154). Cincinnati, OH: American Conference of Governmental Industrial Hygenists (ACGIH).

BGI Inc. (2002). Collison Nebulizer - Instructions. Retrieved from https://bgi.mesalabs.com/wp-content/uploads/sites/35/2014/10/Collison.pdf

Boundary Conditions. (2003) *Fluent 6.1 - User's Guide*. Lebanon, NH: Fluent, Inc.

Bowling, J. (2016). *Challenging the gold standard: alternatives to the collison for aerosol generation in research.* University of Pittsburgh.

Brunekreef, B., & Holgate, S. T. (2002). Air pollution and health. *The lancet, 360*(9341), 1233-1242.

Burgess, W. A., Ellenbecker, M. J., & Treitman, R. D. (2004). *Ventilation for Control of the Work Environment* (Second Edition ed.). Hoboken, New Jersey: John Wiley & Sons, Inc.

CH Technologies. Blaustein Atomizer (BLAM) Multi-Jet Model - User's Manual. Westwood, NJ.

CH Technologies. (2016). Vilnius Aerosol Generator (VAG) - User's Manual (Setup, Operation, and Maintenance). 34.

Chen, B., Yeh, H.-C., & Fan, B. (1995). Evaluation of the TSI small-scale powder disperser. *Journal of Aerosol Science, 26*(8), 1303-1313.

Chen, B. T., Feather, G. A., Maynard, A., & Rao, C. Y. (2004). Development of a personal sampler for collecting fungal spores. *Aerosol science and technology, 38*(9), 926-937.

Chen, B. T., Fletcher, R. A., & Cheng, Y.-S. (2011). Calibration of aerosol instruments. *Aerosol Measurements: Principles, Techniques, and Applications. 3rd. Hoboken NJ: John Wiley and Sons*, 449-478.

Hinds, W. C. (1999). Aerosol Technology: Properties. *Behavior, and Measurement of airborne Particles (2nd*.

Hinds, W. C., & Kuo, T.-L. (1995). A Low Velocity Wind Tunnel to Evaluate Inhalability and Sampler Performance for Large Dust Particles. *Appl Occup Environ Hyg, 10*(6), 549-556. doi:10.1080/1047322X.1995.10389073

Kampa, M., & Castanas, E. (2008). Human health effects of air pollution. *Environmental pollution, 151*(2), 362-367.

Kulkarni, V., Sahoo, N., & Chavan, S. D. (2011). Simulation of honeycomb–screen combinations for turbulence management in a subsonic wind tunnel. *Journal of wind engineering and industrial aerodynamics, 99*(1), 37-45.

Lam, C. W., Scully, R. R., Zhang, Y., Renne, R. A., Hunter, R. L., McCluskey, R. A., . . . James, J. T. (2013). Toxicity of lunar dust assessed in inhalation-exposed rats. *Inhal Toxicol, 25*(12), 661-678. doi:10.3109/08958378.2013.833660

Lee, S., Yu, M., & Kim, H. H. (2013). Development of aerosol wind tunnel and its application for evaluating the performance of ambient PM10 inlets. *Atmospheric Pollution Research, 4*(3), 323-328. doi:http://dx.doi.org/10.5094/APR.2013.036

Li, Z., Chapman, R., Malinin, V., Corboz, M., Gauani, H., Laurent, C., . . . Plaunt, A. (2017). Pharmacokinetic (PK) Comparison Between Nebulized And Dry Powder INS1009 In Rats *B71. PULMONARY HYPERTENSION LIFE: ANIMAL MODELS AND EX VIVO STUDIES IN PULMONARY HYPERTENSION* (pp. A4200-A4200): Am Thoracic Soc.

Lindsley, W. G., Schmechel, D., & Chen, B. T. (2006). A two-stage cyclone using microcentrifuge tubes for personal bioaerosol sampling. *Journal of Environmental Monitoring, 8*(11), 1136-1142.

Liu, Xiao. (2018). *Validation of a New Concept for Measuring Respirable Dusts*. University of South Florida. Unpublished Manuscript.

Lodge, J. P., Pate, J. B., Ammons, B. E., & Swanson, G. A. (1966). The Use of Hypodermic Needles as Critical Orifices in Air Sampling. *Journal of the Air Pollution Control Association, 16*(4), 197-200. doi:10.1080/00022470.1966.10468462

May, K. (1973). The Collison nebulizer: description, performance and application. *Journal of Aerosol Science, 4*(3), 235IN1239-238243.

Mehta, R. D., & Bradshaw, P. (2016). Design rules for small low speed wind tunnels. *The Aeronautical Journal (1968), 83*(827), 443-453. doi:10.1017/S0001924000031985

National Research Council. (2006). *Overcoming Challenges to Develop Countermeasures Against Aerosolized Bioterrorism Agents: Appropriate Use of Animal Models*: National Academies Press.

Occupational Safety and Health Administration. (1995). Asbestos Standard for General Industry. Retrieved from https://www.osha.gov/Publications/osha3095.html

Occupational Safety and Health Administration. (2017). 1910.1053 - Respirable Crystalline Silica. Retrieved from https://www.osha.gov/silica/SilicaGeneralIndustryRegText.pdf

Pieretti, Luis F., "Characterization and Evaluation of Performance of a Whole-Body Human Exposure Chamber" (2010). *Graduate Theses and Dissertations.* http://scholarcommons.usf.edu/etd/3611.

Plog, B. A., & Quinlan, P. J. (2002). *Fundamentals of Industrial Hygiene* (5th ed.): National Safety Council.

Pope III, C. A., & Dockery, D. W. (2006). Health effects of fine particulate air pollution: lines that connect. *Journal of the Air & Waste Management Association, 56*(6), 709-742.

Raabe, O. G. (1968). The dilution of monodisperse suspensions for aerosolization. *Am Ind Hyg Assoc J, 29*(5), 439-443. doi:10.1080/00028896809343031

Ramachandran, G., Sreenath, A., & Vincent, J. H. (1998). Towards a new method for experimental determination of aerosol sampler aspiration efficiency in small wind tunnels. *Journal of Aerosol Science, 29*(7), 875-891.

Reed, D. S., Xhillari, D., Weiss, A. L., & Jaeger, R. J. (2016). Aerosol Exposure to Pathogenic Bacteria and Virus Particles: Standard Operating Procedure *Aerobiology* (pp. 445-459).

Riley, Laura, "Expansion of the Performance Capabilities of the USF Inhalation Challenge Chamber" (2016). *Graduate Theses and Dissertations.* http://scholarcommons.usf.edu/etd/6575.

Rissler, J., Asking, L., & Dreyer, J. K. (2009). A methodology to study impactor particle reentrainment and a proposed stage coating for the NGI. *J Aerosol Med Pulm Drug Deliv, 22*(4), 309-316.

Rissler, J., Gudmundsson, A., Nicklasson, H., Swietlicki, E., Wollmer, P., & Löndahl, J. (2017). Deposition efficiency of inhaled particles (15-5000 nm) related to breathing pattern and lung function: an experimental study in healthy children and adults. *Particle and fibre toxicology, 14*(1), 10.

Scheiman, J., & Brooks, J. (1981). Comparison of experimental and theoretical turbulence reduction from screens, honeycomb, and honeycomb-screen combinations. *Journal of Aircraft, 18*(8), 638-643.

Schmees, D. K., Wu, Y.-H., & Vincent, J. H. (2008). Experimental methods to determine inhalability and personal sampler performance for aerosols in ultra-low windspeed environments. *Journal of Environmental Monitoring, 10*(12), 1426-1436.

Scully, R. R., Lam, C. W., & James, J. T. (2013). Estimating safe human exposure levels for lunar dust using benchmark dose modeling of data from inhalation studies in rats. *Inhal Toxicol, 25*(14), 785-793. doi:10.3109/08958378.2013.849315

Seaton, A., Godden, D., MacNee, W., & Donaldson, K. (1995). Particulate air pollution and acute health effects. *The lancet, 345*(8943), 176-178.

Siddique, S. A. (2012). *Design, Development, and CFD Validation of a Subsonic Wind Tunnel*. Paper presented at the Student Professional Development Conference (SPDC), Toledo, OH.

Singh, N. S. (2013). Review of Design and Construction of an Open Circuit Low Speed Wind Tunnel. *Global Journal of Researches In Engineering, 13*(5).

Stairmand, C. (1941). Sampling gas-borne particles. *Engineering, 152*, 141-143, 181-183.

Su, W.-C., Tolchinsky, A. D., Chen, B. T., Sigaev, V. I., & Cheng, Y. S. (2012). Evaluation of physical sampling efficiency for cyclone-based personal bioaerosol samplers in moving air environments. *Journal of Environmental Monitoring, 14*(9), 2430-2437.

The New York Blower Company. (2013). Compact GI Fans with Rugged Radial-Blade Wheels. Retrieved from http://www.nyb.com/Catalog/Bulletins/231.pdf

The Sherwin Williams Company. (2015). General Polymers 3525 - Static Control Epoxy Coating. Retrieved from http://generalpolymers.com/drop/3525.pdf

Thermo Fisher Scientific. (2018). *Particle Technology Technical Notes and Reference Guide - Strategies and Procedures for Bead Optimization*. Retrieved from Fremont, CA: https://assets.thermofisher.com/TFS-Assets/CDD/Catalogs/CAT-10021654-PT-TECH-GUIDE-EN.pdf

United States Department of Energy. (2003). *Nuclear Air Cleaning Handbook*. Retrieved from https://energy.gov/sites/prod/files/2013/09/f3/chapter8_1.pdf

United States Environmental Protection Agency. (2016a). 40 CFR 53.62 - Test Procedure: Full Wind Tunnel Test. Washington, DC: United States Government Publishing Office

United States Environmental Protection Agency. (2016b). Health and Environmental Effects of Particulate Matter (PM). Retrieved from https://www.epa.gov/pm-pollution/health-and-environmental-effects-particulate-matter-pm

Wagner, J., & Leith, D. (2001). Passive aerosol sampler. Part II: Wind tunnel experiments. *Aerosol Science & Technology, 34*(2), 193-201.

Yi, J., Chen, B. T., Schwegler-Berry, D., Frazer, D., Castranova, V., McBride, C., . . . Nurkiewicz, T. R. (2013). Whole-body nanoparticle aerosol inhalation exposures. *Journal of visualized experiments: JoVE*(75).

Zhen, H., Han, T., Fennell, D. E., & Mainelis, G. (2014). A systematic comparison of four bioaerosol generators: Affect on culturability and cell membrane integrity when aerosolizing Escherichia coli bacteria. *Journal of Aerosol Science, 70*, 67-79.

Appendices

Appendix A – USF IRB Exemption Letter

USF
UNIVERSITY OF
SOUTH FLORIDA

RESEARCH INTEGRITY AND COMPLIANCE
Institutional Review Boards, FWA No. 00001669
12901 Bruce B. Downs Blvd., MDC035 • Tampa, FL 33612-4799
(813) 974-5638 • FAX(813)974-7091

2/12/2018

Jason Garcia
Environmental and Occupational Health
13201 Bruce B. Downs Blvd. MDC 56
Tampa, FL 33612

RE: **Not Human Subjects Research Determination**
IRB#: Pro00034156
Title: Design, Construction, and Characterization of the University of South Florida Wind Tunnel

Dear Mr. Garcia:

The Institutional Review Board (IRB) has reviewed your application. The activities presented in the application involve methods of program evaluation, quality improvement, and/or needs analysis. While potentially informative to others outside of the university community, study results would not appear to contribute to generalizable knowledge. As such, the activities do not meet the definition of human subject research under USF IRB policy, and USF IRB approval and oversight are therefore not required.

While not requiring USF IRB approval and oversight, your study activities should be conducted in a manner that is consistent with the ethical principles of your profession. If the scope of your project changes in the future, please contact the IRB for further guidance.

If you will be obtaining consent to conduct your study activities, please remove any references to "research" and do not include the assigned Protocol Number or USF IRB contact information.

If your study activities involve collection or use of health information, please note that there may be requirements under the HIPAA Privacy Rule that apply. For further information, please contact a HIPAA Program administrator at (813) 974-5638.

Sincerely,

V Jorgensen MD

E. Verena Jorgensen, M.D., Chairperson
USF Institutional Review Board

Appendix B – Nitrogen Gas Cylinder Regulator Calibration Curve

Breath Lab N_2 Gas Cylinder Pressure Regulator Calibration Curve		
Pressure (psi)	**Flow Rate (LPM)**	**Average Flow Rate (LPM)**
10	3.28	3.22
	3.16	
	3.21	
15	4.56	4.65
	4.73	
	4.66	
20	5.94	5.93
	5.94	
	5.90	
25	7.10	7.08
	7.09	
	7.04	
30	8.18	8.17
	8.18	
	8.14	
35	9.43	9.38
	9.34	
	9.36	
40	10.44	10.42
	10.45	
	10.37	

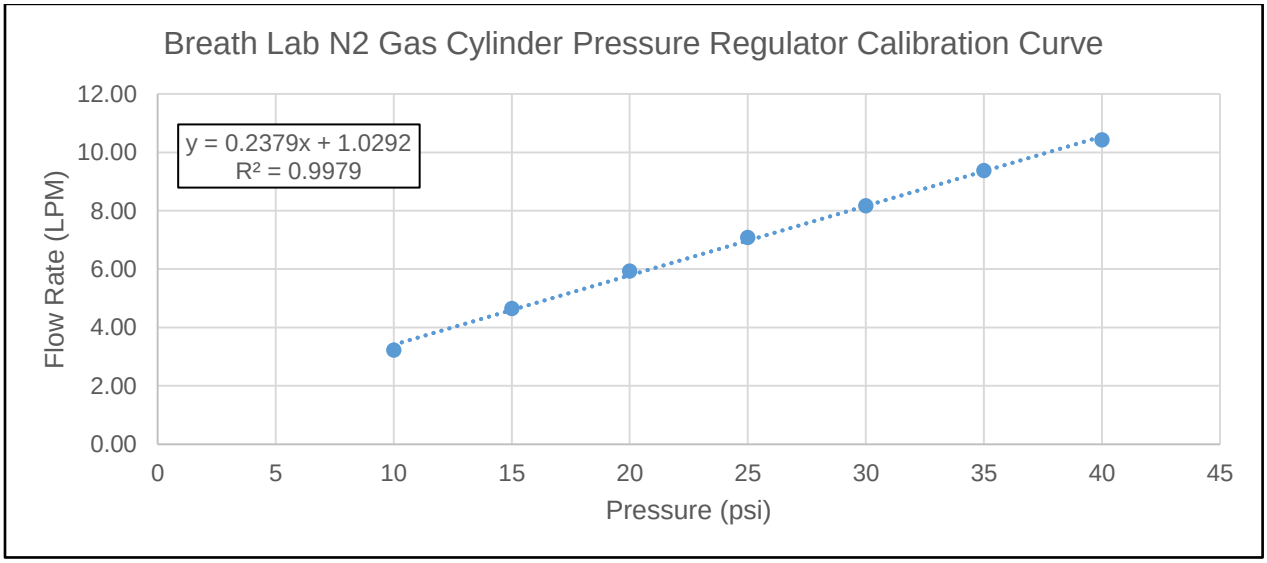

Appendix C – Thermo Fisher Scientific, Inc. Permission

COPYRIGHT PERMISSION

REPRESENTATIONS

A. Thermo Fisher Scientific Inc., with a location at 168 Third Street, Waltham, Massachusetts 02451 ("Thermo Fisher") owns the copyrights to a publication entitled *"Particle Technology. Technical Notes and Reference Guide"* published in 2018, which includes a graph labelled "Figure 3. Thermo Scientific Red Fluorescing Particles" on page 54, as shown on Appendix 1 attached to this document (the "Figure").

B. Jason S. Garcia, an individual and doctoral candidate in Industrial Hygiene, College of Public Health, University of South Florida ("Garcia"), seeks permission to use the Figure in his doctoral dissertation (the "Purpose"), and Thermo Fisher is willing to grant such permission in accordance with the terms set forth below.

THEREFORE:

1. Thermo Fisher hereby authorizes Garcia to copy and use the Figure solely in connection with the Purpose, including the right to publish, print, reproduce, combine with other images or content, distribute, or otherwise use the Figure in any form or medium, including electronic or printed copy, as may be required in connection with the Purpose.

2. Thermo Fisher represents that it owns the entire right, title and interest in and to the Figure and has the right to grant to Garcia permission to use the Figure as provided herein. No other rights or interest shall pass to Garcia and Thermo Fisher shall retain full ownership of the copyrights to the Figure.

3. Thermo Fisher shall not be compensated monetarily. However, Garcia shall acknowledge Thermo Fisher when using the Figure, for example: "Figure provided courtesy of Thermo Fisher Scientific."

Agreed:

THERMO FISHER SCIENTIFIC INC.

By: _____

Name: Denise Riemann

Title: Sr. Intellectual Property Counsel

Date: June 14, 2018

JASON S. GARCIA

By: _____

Name: JASON S. GARCIA

Title: DOCTORAL CANDIDATE - UNIVERSITY OF SOUTH FLORIDA

Date: 6/15/18

APPENDIX 1

The Figure

Figure 3. Thermo Scientific Red Fluorescing Particles

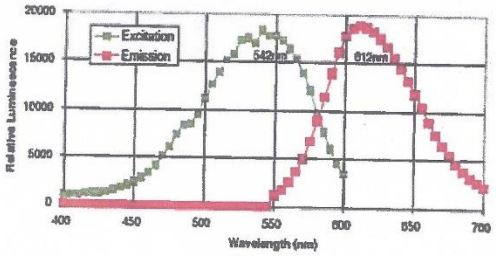

Appendix D – Xiao (Sarah) Liu Permission

Red Fluorescent Polystyrene Latex Sphere Calibration Curve Permission

Garcia, Jason

Thu 6/14/2018 12:42 PM

Sent Items

To: Liu, Xiao <xliu1@health.usf.edu>;

Importance: High

Hey Sarah,

Since I used the same calibration curve that you did for my dissertation research, I would like to put a copy of it in my dissertation document. Even though we both worked on it, you were the one that created the final product. In order to abide by university guidelines and copyright laws, I'm responsible for asking for permission to use it since my dissertation will be made openly accessible online through our institutional repository.

Do I have your permission to put the "Red Fluorescent Polystyrene Latex Sphere Calibration Curve" in my dissertation document?

Please respond back to this e-mail with your answer. Thanks!

Best regards,

Jason S. Garcia, MPH, CPH
Doctoral Candidate - Industrial Hygiene
University of South Florida
College of Public Health
13201 Bruce B. Downs Blvd, MDC 56
Tampa, Florida 33612
1-863-990-1330
jgarcia4@health.usf.edu

"Limits, like fear, are often just an illusion." - Michael Jordan

Re: Red Fluorescent Polystyrene Latex Sphere Calibration Curve Permission

Liu, Xiao

Thu 6/14/2018 4:45 PM

To: Garcia, Jason <jgarcia4@health.usf.edu>;

Cc: Hammad, Yehia <yhammad@health.usf.edu>;

Hi Jason,

Yes, you can include the "Red Fluorescent Polystyrene Latex Sphere Calibration Curve" in your dissertation.

Sarah Liu

Sent from phone